STUDY OF DISPERSION PHENOMENON IN CREUSOT LOIRE UDDEHOLM REACTOR

Kabezya Kitungwa

A Dissertation submitted to the Faculty of Engineering and the Built Environment, University of the Witwatersrand, in fulfillment of the requirements for the degree of Master of Science in Engineering.

Johannesburg, 2008

DECLARATION

I declare that this thesis is my own, unaided work. It is being submitted for the Degree of Master of Science in Engineering in the University of the Witwatersrand, Johannesburg. It has not been submitted before for any degree or examination in any other University.

Kabezya Kitungwa

Date :28 May 2008

ABSTRACT

A study on the slag dispersion in bath smelting converter was undertaken. The aim was mainly to investigate the behaviour of the dispersed slag phase at high gas flow rate and low slag volume (10%) systems. For simulations purposes, water; paraffin-oil and air were used in a one fifth model of the commercial 100 ton Creusot-Loire-Uddeholm converter to represent bulk steel, molten slag and gas respectively. Emulsion samples were collected by means of the specially made syringe. The experimental results revealed that the dispersed slag phase decreased with the vertical distance from the original interface between the liquid phases. The dispersed phase decreased also with the radial distance in the water plume zone towards the wall side. The holdup was apparently much observable on the right side than on the left side. Four dimensionless numbers defined the dispersion phenomenon through the dimensional analysis. The modified Froude Number ensured the correlation between both model and prototype. The standard error of the estimate and R-squared between the experimental and the calculated results were 3.7×10^{-4} and 0.97 respectively.

ACKNOWLEDGEMENTS

The author would like to thank Professor Eric for the supervision and guidance of the current work. Financial support provided by Columbus steel is gratefully acknowledged. The author is also indebted to the following services; workshop and cleaning. Thanks go to Professor Kucukkaragoz for encouragements. Special thanks to my colleagues who shared the pyrometallurgical laboratory with me.

CONTENTS Page

LIST OF TABLES

Table **Page**

LIST OF FIGURES

Figure **Page**

LIST OF SYMBOLS

V_o	Volume of oil in the sample emulsion
V_w	Volume of water in the sample emulsion
Dph	Dispersed phase holdup
G	Acceleration due to the gravity
μ	Dynamic viscosity
z	Axial distance from the original interface
r	Radial distance
H_o	The height of oil in the bath before air injection
H_w	The height of water in the bath before air injection
ρ	Density
v	Velocity of gas flow rate at the nozzle tip
Fr	Froude Number
N_{Fr}	Modified Froude Number
CLU	Creusot Loire Uddeholm
L	Length
M	Mass
T	Time
Q	Volumetric gas flow rate
d	Nozzle diameter
u	Nominal velocity at the nozzle tip
AOD	Argon – Oxygen-Decarburization
$meas$	Measure
R^2	R-squared
BOF	Basic oxygen furnace

1 INTRODUCTION

1.1 Emulsions in bath smelting

1.1.1 Definitions

From literature survey, the word emulsion could be defined differently, according either to the movement of droplets or to the nature of phase [1, 2] .Emulsions are systems consisting of small liquid droplets or gas bubbles imbedded in a liquid medium when the distances separating the neighboring droplets (liquid/liquid) or bubbles (gas/liquid) are large enough to allow the independent movement of the said droplets or bubbles. When the volume of the liquid medium in a gas/liquid emulsion is small as compared with the volume of the gas bubbles, the medium will be present only in the form of thin film separating the adjacent bubbles, these cannot move freely and the whole system is then called foam. Hence, emulsions are dispersed multi-phase systems of two or more insoluble liquids. They consist of at least one continuous (outer) phase (e.g. water) and one isolated (dispersed or inner) phase (e.g. oil) [3].Thus, emulsions are heterogeneous systems formed by immiscible liquids closely dispersed in another in droplet form [4]. Lin and Guthrie [5] defined emulsion as a result of the dispersion of one liquid in another one. The size distribution of the emulsion is described via a typical mean diameter based on statistical moments. The mean surface diameter or Sauter diameter, d_{32}, is the more relevant one in cases where the interfacial area is a control parameter for the mass transfer or chemical reaction: it is used extensively in the characterization of liquid/liquid or gas/liquid dispersions [4].

1.1.2Types of emulsions

Emulsion can be classified according to the size of droplet and to the nature of the dispersed phase.

- Based on the size of liquid drop, two types of emulsions are possible:

(a) Macro emulsions when the particles range from 0.2 to 50 micrometers in size and are visible under microscope.

(b) Micro emulsion has particles from 0.01 to 0.20 micrometer.

Fine drop production in gas liquid-liquid system was found to come from three distinct sources such as; the disintegration of liquid columns entrained by bubbling gas as they cross the liquid-liquid interface, drop erosion during collisions with gas bubbles and multiphase drop rupture at the upper liquid-gas interface [6,61].

- Based on the nature of the dispersed phase, two types of emulsions are also distinguished namely:

(a) Oil in water; inverse (or reverse) emulsification

(b) Water in oil; normal emulsification.

The type of emulsion formed by the water/oil system depends on the operating conditions such as; gas flow rate, the relative proportions of oil and water and much more on the blowing location (top, bottom or combined).

Number of researchers has gathered evidence on the nature of emulsion in steel making converters. Tanaka and Guthrie [7] reported normal emulsification in top blowing process and inverse emulsification in combining blowing. On the other hand, Z.Lin and Guthrie [5] observed two types of emulsion according to the nature of dispersion. Normal emulsion was also observed in the simulation of the LD process, in the top blowing. The thickness of the emulsion formed increased by positioning the lance nearer to the bath surface [8]. One type can be converted into another by manipulating operating conditions such as the height ratio of liquid phases.

1.1.3 Formation of emulsion.

The emulsification of metal may be due to the mechanical energy supplied by blowing and by decarburization. The bath agitation plays a major role in the formation of emulsion. The more the gas flow rate increases, the greater the speed of emulsification will be [8]. But the emulsion collapses when the equilibrium approaches because it is thermodynamically unstable [9].

In steel making with oxygen top blowing, as in the B.O.F and some C.L.U processes, entrainment of metal droplets in slag is caused both by the impact of the oxygen jet and carbon monoxide evolution from the metal bath [10,73]. Anyhow, there are three different ways where a metal in slag emulsion can be formed in C.L.U reactor [1]:

- Direct dispersion of the metal in slag
- Decomposition of a chemical compound dissolved in the slag
- Separation, on cooling metal initially dissolved in the slag.

Poggi *et al* [11] recognized on the other hand that the important mechanism of metal transport into slag is through bubbles rising across the metal/slag interface. The present work focuses on the first way. Generally, in the formation of emulsion, one of the immiscible phases is broken up into particles that are dispersed in the other phase. The dispersion of the inner liquid causes an increase in the interfacial area creating a large increase in the interfacial free energy of the system [12].

E.Fritz and G.Gebert [13] argued that the emulsion in high temperatures converters is the result of the formation of large amounts of carbon monoxide in contact with the liquid slag and metal droplets.

1.1.4 Mechanisms of the droplet formation

Z.Han and L.Holappa [14] investigated the physical phenomena occurring during the passage of single bubbles through the iron/slag interface by means of x-ray transmission technique and optical microscopy. From their observations, two different groups of droplets were pointed out during the passage of a big bubble through the iron /slag interface, namely jet and film entrainment. Lin and Guthrie [7] found that droplet formation was the effect of the density and the gas injection .At lower gas rate, droplet formation is due to the interfacial instability whereas at high gas flow rate, droplet birth is the result of gas bubbles with the liquid phase. Distinct systems were used in their investigations such as; oil/$ZnCl_2$, oil/water.

Drop formation in the CLU vessel is the consequence of liquid deformation due to the direct effect of uprising bubbles. Drops disintegrate into droplets during the blowing process due to the intensity of the following factors; swirling, waves, vortices, eddy size and shear stress. Frohberg and Handshuh [15] argued that the blowing time is the key factor in the mechanism of drop formation. On the other hand, Martin, *et al* [16] asserted that the droplet generation was governed by two factors namely the intensity of the movement of the gas jet on the surface of the bath, and the physical properties of the liquid.

1.1.5 Stability of emulsions

Owing to the fact that the emulsification is an interfacial phenomena, the stability of emulsions in the commercial C.L.U depends a great deal on physical properties of the surface film between metal and slag such as [9]:

- High viscosity of the slag

When the slag viscosity is high, the surface tension is considerable to such an extent that the entrapment of metal in slag is more important. It is known that the slag viscosity increases with silica content [1]

- Adherence of solid particles to the surface of bubbles and drops

The stability may be due to sticking of solid particles to the bubbles surface when there is partial crystallization in the reactor

• Adsorption phenomena.

Kozakevitch [1] pointed out the adsorption of some cations at the surface film formed by silica in the form of an ionic double layer.

Adsorption of any solute at the surface is given by Gibbs equation as follows:

$$\tau = -\frac{a}{RT}\frac{d\gamma}{da} \qquad [1]$$

Where: Γ represents the adsorption, it is positive or negative (depletion)

γ, the surface tension of a liquid solvent

a, the thermodynamic activity of the solute in the bulk

R is the gas constant

T is the absolute temperature

• Inhibition of drop movement or gas bubbles within the emulsion

In B.O.F. steel making and in C.L.U refining, coalescence of two droplets is improbable in the presence of carbon monoxide bubbles, a gaseous film preventing direct contact when there is large carbon monoxide evolution inside the emulsion [9]. However, the destruction of emulsion can be observed either by coalescence and sedimentation, or by complete combustion.

• Temperature

At constant temperature, the interfacial tension between slag and metal and the viscosity of the interfacial film don't change in the nature [17].

•Size distribution

An emulsion with uniform size distribution is more stable than one having a wider distribution with the same average, since the size distribution is a function of the residence time of droplets.

1.1.5.1 Stabilization and destruction of the emulsion

In aqueous modeling techniques, emulsion is generated by the effect of gas injection (top, bottom and combined blown) and collapses once the blowing process is stopped. In high temperature converters, the reaction of carbon and oxygen produces carbon monoxide that plays the key role in stabilizing slag-metal emulsion. Coalescence of droplets is quite improbable as long as carbon monoxide is adhered on the surface of slag or metal droplet [9]. Coalescence is the opposite effect of dispersion. Drops recombine when the kinetic energy of their relative motion is smaller than their energy of adhesion [18].

1.15.2 Instability of the original interface

The original interface is the surface formed by immiscible fluids before gas injection. The form of the original interface depends upon the following physical factors,

- Physical properties of the fluids
- The hydrostatics features of fluids such as pressure of the top phase on the denser phase and resultant buoyancy.
- The original interface is parallel to the nozzle side in the CLU vessel

Different types of instabilities may occur on the original interface during the emulsification process, depending upon the hydrodynamics of fluids [*18, 68*, and 71].
To illustrate such instabilities, the following may be cited;
1) Tollmien-Schlichting instability that is observable when the inertial dynamical forces are superior to viscous forces.
2) Kelvin-Helmholtz instability that is due to the gradient of tangential velocities of distinct fluids across the original interface.
3) Rayleigh-Taylor instability that is observed when the movement of the original interface is directed from the lighter phase towards the dense phase.
4) Bernard instability occurs in case of adverse density gradients of fluids.

1.1.6 Importance of emulsions in CLU reactor

- The formation of emulsion in the CLU converter enhances the contact between the phases. Accordingly, mass transfer and heat transfer are favoured [8].
- The formation of a large metal/slag interfacial area responsible for the high reactions rates [19].
- The bath temperature will increase dramatically in the absence of emulsions reactions [20].
- Meyer, *et al* [21] estimated that almost 60 % of carbon removal occurred via emulsion.
- Martin, *et al* [16] emphasized that an insufficient emulsion may cause an increase in the refining time.

The overall reaction rate (N) is generally expressed by the following equation;

$$N = kA\Delta C \qquad [2]$$

Where, k represents the reaction rate constant. It is dependent on chemical reaction and liquid mass transport.

A, is the total interfacial area.

ΔC , is the difference of activities.

Earlier work [22] emphasized on the fact that the interfacial area created by the gas injection is the major phenomena affecting the kinetics of reactions and mass transfer.

During the smelting process, high heat and mass transfer rates occur as a result of the intense mixing and large interface developed between metal and slag [23, 24].The formation of slag-metal emulsions is of considerable practical importance in pyrometallugy particularly during the refining stage. These emulsions create large interfacial area between slag and molten metal resulting in rapid chemical reactions and mass transfer rates encountered in bath smelting, in the Basic Oxygen Furnace (BOF), in the Q -B.O.P. and in the commercial C.L.U converter.

The current work is divided into two parts. The first one aimed at the literature review of metallurgical emulsions in order to better develop a physical model of dispersion phenomena of the Creusot–Loire–Uddeholm (C.L.U) reactor. The second part outlines the experimental work.

From literature survey, previous studies have been concentrated on liquid –liquid emulsions of low gas flow rate- low slag volume or high gas flow rate / high slag volume. The objective of this study was to investigate the dispersion behaviour in high gas flow rate –low slag volume operations. Then, the other purpose of this work was to build up a mathematical model of the dispersed phase in order to extrapolate the experimental results to the industrial scale.

Similarity between the model and the prototype was ensured by the modified Froude number criterion. For simulation purposes, a water model of CLU converter was utilized in order to characterize the dispersed phase hold up in high strength bottom blown reactors for various injection rates and water-paraffin oil heights.

2 LITERATURE REVIEW

2.1 AOD, CLU processes.

Nowadays, stainless steelmaking is achieved efficiently through technologies like AOD (Argon-oxygen-decarburization) and CLU (Creusot-Loire-Uddeholm).Both processes are similar in their applications. The difference lies on the gaseous mixture used and the location of gas injection.

Figure1: The commercial CLU converter

The charge of the CLU or AOD converter is composed of the hot metal from the arc furnace, fluxes and others additions such as scrap and ferro-chromium. The hot metal (crude steel) contains mostly iron, chromium, nickel, carbon and other undesirable elements such as phosphorus, sulfur and manganese. Fluxes are salts that are added to the bath for the purpose of slagging undesirable elements and balancing the heat

within the bath at the optimum level. Hot metal is formed mostly by scrap. Fluxes are dependent on the chemical nature of the slag (acid or alkaline) and the refractory wear.

The gas mixture is injected through nozzles or tuyeres located at or near the bottom of the vessel to promote mixing, heat transfer and mass transfer in the bath smelting. Under these conditions; reactions take place rapidly resulting in a higher refining rate. As reactions proceed, three phases are formed in the bath namely molten steel, liquid slag and gas. The lighter phase (slag) floats on top of the heavier phase (molten steel) during the refining process. The gas mixture characteristics used in AOD and CLU are given in Table 1.

Table1: Gas injection characteristics in AOD and CLU

Process	Bottom gases	Tuyere location
AOD	Oxygen Argon Nitrogen Carbon monoxide	Side - bottom
CLU	Steam, Argon, Nitrogen Oxygen	Bottom

South African Columbus Steel uses the commercial CLU converter equipped with a top lance (combined blowing) as shown in figure1.In both processes; the ratio of inert gas to oxygen is enhanced to promote decarburization without excessive chromium oxidation [24].

The usefulness of the converter comes from its ability in producing low carbon stainless steel. Steam is used in the CLU process for thermodynamic requirement as a

temperature controller and for inhibiting chromium oxidation. Also; the steam is utilized for the sake of reducing inert gas (Ar) consumption [25, 60, and 69].

2.2 Previous work

Number of investigations on metallurgical emulsions has been performed on the bottom, top and combined gas blowing liquid-liquid systems.

Tanaka and Guthrie [7] studied emulsification phenomena in liquid –liquid systems using water-paraffin, mercury-paraffin and mercury-glycerin systems, respectively. The aim of their investigation was to investigate the slag entrainment by steel during simulation blowing operations in steelmaking. A 1:19th scale model of 240 ton BOF steelmaking vessel was used in two systems; water-paraffin and mercury/paraffin. Normal emulsion (water droplets in the oil layer) was observed in top blown. Whereas in bottom blown, they reported the inverse emulsion (oil droplet in the water).The combination of top and bottom blowing enhances the entrainment of particles.

Investigations on the control of reverse emulsification in a bottom blown bath were undertaken by means of a circular plate by S.Yamashita and M.Manachu [26]. They found that as the plate approached the bottom side, the dispersion of slag droplets increased in the whole bath and the mixing time was shortened. In case where the circular plate was removed, the recirculating flow diminished.

Martin and M.Diaz [27, 8] investigated the hydrodynamics of gas-liquid and gas-liquid-liquid reactors with top and bottom blowing. The reactor consisted of a cold model of a 250-ton industrial converter and the triple system water-Vaseline-air. The aim of their study was to characterize the bubbles and to determine the streamlines, the study of drops and emulsions formed. Their results described the fluid dynamics of the gaseous phase and aqueous phase.

R.P. Singh and D.N.Ghosh [28] carried out a cold model study of liquid-liquid mass transfer (Water/ benzene model) in a combined blowing converter under experimental conditions such as bottom gas flow rate, number of tuyeres and dimensionless radial positions. The modified Froude Number was adjusted for the water model to simulate plant scale operation. The improvement realized in the combined blowing process was attributed mainly to enhanced emulsification of benzene in water.

Zaidi and Sohn [29] investigated liquid-liquid formed by bottom gas injection to characterize the drop size distribution using kerosene-water system at gas flow rates ranging from 54Nl/min to 282 Nl/min for a slag volume of 33-75%.A polycondensation technique was used to collect sample of the dispersed water drop, by means of a specially designed pneumatic trap. The drop-size distribution was found to obey the Gaudin-Schulmann equation. In light of size distribution of the drops, M.G.Frohberg and G.Handschuh [15] studied the emulsion in bottom converter. They observed that the distribution peaks changed to smaller diameters by increasing the blowing time.

D.J.Phelan and G.Brooks [23] investigated coalescence and breakage of sulphide matte droplets in the slag-matte emulsions of the Vanyukov process. The gas flow rates ranged from 0 to 40 Nl/min.The mean droplet diameter was found to increase with the gas flow rates.

Turkdogan [10, 30] observed photographically the phenomena of emulsion formation aimed at the mechanism of formation of metal droplets dispersed in slag of open – hearth steel making processes and more importantly in B.O.F.In these processes, metals droplets are formed and dispersed in the slag layer due to the impinging gas jets, as well as rising gas bubbles. It was found that at low impinging gas jet velocities, no emulsification was observed, while at high jet momentum, oil and water layers became emulsified at the interface.

Wei and Oeters [31] investigated the emulsion in the injection ladle using water and cyclohexane to model the liquid steel and slag respectively. It was found that the number of droplets of slag increased with increasing stirring gas flow rate, but the average diameter of droplets decreased and the location of the nozzle used influenced the number of droplets generated

W.Kleppe and F.Oeters [32] conducted model tests on the breakaway of droplets when blowing a gas jet onto the surface liquid. A model law describing the dispersion formation in basic oxygen process was defined in the absence of a slag layer. They asserted that the basic oxygen process takes place in atomization range.

B.Deo *et al* [33] investigated slag-metal droplet emulsion in oxygen steelmaking. An emulsion number was defined on the basis of the residence time of metals droplets and gas bubbles found in liquid slag. The so-called emulsion number was qualified to be a probable tool in controlling slag formation.

On the other hand, Subagyo *et al* [34] carried out investigations aimed to the study of the behavior of metal droplets in slag-metal emulsion through impinging gas blowing. They found out that the generation rate and size distribution of metal droplets was effected by the blowing number.

G.Brooks *et al* [35] developed a model of trajectory and residence time of metal droplets in slag-metal –gas emulsion. Their model based on mechanics and chemical kinetics principles showed that the residence time of metals droplets in slag was short for a weakened decarburization in oxygen steelmaking.

G.Reiter and K.Schwerdtfeger [36] investigated the physical phenomena occurring during passage of bubbles through the liquid/liquid interfaces. By means of the high speed photography, they observed that the bubble spends a time at the interface before it reaches the upper phase. On the other hand, the denser phase dragged upwards increased with bubble size.

Z.Han and L.Holappa [14] carried out investigations on the mechanism of the entrainment at the iron/slag interface. They used X-ray transmission technique and optical microscopy. They attributed the iron entrapped into slag to jet and film entrainment.

D.Poggi, *et al* [11] investigated the mechanisms of metal entrained in slag found in Noranda Processes using two systems; mercury/water-glycerin and lead /fused salt. They observed that matte might become entrapped either as rafts of droplets, as droplets suspended or as fine droplets.

P.Kozakevitch [1] carried out investigations on foams and emulsions in steelmaking. The factors responsible of stabilizing foams and emulsions in steelmaking were defined.

Z.Lin and Guthrie [5] studied the emulsification behavior caused by gas bubbles rising through a slag/metal interface using aqueous modeling techniques. Two opposite patterns of emulsion were observed. The first pattern consisted of aqueous droplets dispersed within the oil phase. The second pattern consisted of oil droplets dispersed within the aqueous phase (inverse emulsion).This depended on the system chosen and the operating conditions. For systems of large differential density with a thick upper phase (e.g. in the bath smelting process), it was found that the dispersion of lower phase into the upper phase was more significant than the inverse process. A generalized model characterizing the transitional volume of entrained droplets within the upper phase in the emulsification process was developed. Dimensional analysis was used to express the volume of lower liquid carried up into the emulsion per bubble.

Lee and Sohn [37] carried out a cold model study on the effects of various operating conditions on the dispersed phase holdup in liquid-liquid emulsion generated by bottom gas injection. They used water and kerosene to simulate the dispersion of slag in QSL lead making process. The variation of the hold up within the plume was correlated by a single equation involving a set of dimensionless numbers. They also

established a relation between the interfacial area and the volume fraction of the dispersed phase in order to estimate or correlate the mass and heat transfer rates in designing a reactor.

G.Akdogan and R.Eric [38, 39] carried out a physical modeling study to simulate the slag-metal dispersion induced by a high rate bottom gas in one-seventh model of a CLU converter utilized in ferroalloy refining. The dispersed phase hold up was determined at various axial and radial distances, gas flow rates, and tuyere configurations (off-center, triangular center and center).They found out that off-center configuration presented better dispersion than others.

Most of previous investigations were basically concentrated on other features of emulsion such as nature of emulsion, drop size distribution and drop formation rather the dispersion of one phase in another. Thus, little has been done on the distribution of the dispersed slag phase in bath smelting with respect to the positions and side.

The choice of simulated triphase (water, paraffin and air) used in the current work could be justified firstly by the following reasons;

- The need of inducing the same type of physical phenomena in both reactors (model and prototype)
- To take into account the close physical similarity [27].
- Also, the choice of room temperature model was motivated by the sake of visualizing the physical phenomena occurring in the commercial CLU converter.

On the other hand, D.J.Phelan and Brooks [23] justified the choice of those materials by the physical criteria such as density, viscosity and surface tension. Fabritius et al [24] emphasized that the simulation of the steel phase by water in the isothermal cold model is founded on the nearly equal kinematics viscosity of water and liquid steel.

2.3 Fluid flow in the CLU converter

Fluid flow plays a major role in the CLU converter since all physical phenomena occurring within the bath depend on fluid patterns. Fluid flows are dependent on the following factors; density, interfacial tension, injection regime and bath height. Szekely [40] classified the injection regime in submerged converters in two groups namely;

1) Discrete regime: occurs at lower flow rate, with a characteristic of discrete bubbles.

2) Jet regime occurs at higher flow rate, continuous bubbles are generated. Thus, intensity of bath agitation or turbulence is governed by the injection regime.

Interfacial tensions are forces that force two fluids to remain in contact. These surface tensions delay the movement of one fluid on another in the converter at low gas flow rate as well as in the absence of agitation. Interfacial tension is dependent on the physical nature of fluids (viscous or smooth).

2.4 Similarity criteria and Mathematical modeling

2.4.1 Physical criteria

The development of a physical model of a real operating system called the prototype can make sense only when the model and the prototype are physically similar [40]. In order to achieve the goal of the present work in constructing a model of slag-metal dispersion in the commercial C.L.U, three states of similarity are defined as illustrations but only geometric and dynamic criteria are relevant in the current work. The states of similarity are geometric, dynamic and kinematics.

(a) Geometric similarity relates to the shape of the vessel. The model and the prototype are geometrically similar when the ratio or scale factor of corresponding lengths is the same everywhere

Geometric similarity can be better understood through the theorem of Euclid as follows [41]:

"A pair of plane polygons is similar when they have the same number of vertices and when both of the following conditions are satisfied:

Corresponding angles are in a constant ratio

Corresponding sides are in a constant ratio "

e.g. for 1/5 model of 100ton- C.L.U converter, the scale factor is 5.

$$\frac{H_{CLU}}{H_{Model}} = \frac{L_{CLU}}{L_{Model}} = \frac{D_{CLU}}{D_{Model}} = 5 \qquad [3]$$

Where, H, L and D represent the height, the length and the diameter of the vessel respectively.

(b) Kinematics similarity is the analogy of motion.

(c) Dynamic similarity

Systems are dynamically similar when the magnitudes of forces at corresponding locations are in fixed ratio. There are many dimensionless numbers which are used in dynamic similarity. For example; Reynolds number is the ratio between the inertial forces to viscous force,

$$\mathrm{Re} = \frac{\rho_g U_{nom} L}{\mu} \qquad [4]$$

Where ρ_g is the (gas) density, U_{nom} is nominal velocity, L is the length of the plume and μ is the viscosity of (the gas)

Reynolds number characterizes the laminar or the turbulent nature of the gas jet [42].

Another the criterion which is of great importance in the dynamic similarity of the gas injection onto the liquid surface of metallurgical converter is the Weber number. It is defined by the following relationship

$$We = \frac{\rho_g U^2{}_{nom} L}{\sigma} \qquad [5]$$

Where, σ is the interfacial tension, U is the nominal gas velocity at the nozzle exit, L is the characteristic length and ρ_g is the gas density.

Weber number characterizes the atomization of liquids and bubble/droplet formation Zaidi and Sohn [29] suggested a correlation of Sauter mean diameter (d_{32}) against Weber number for liquid –liquid emulsions formed by bottom gas injection as below,

$$d_{32} = aWe^{0.158} \exp(-0.248We) \qquad [6]$$

Where, We is the Weber number, a is the interfacial area per unit volume of emulsion.

The interfacial area per unit volume of the emulsion is linked to the dispersed slag phase (ϕ) and the mean drop size (d_{32}) by the following the relationship,

$$a = \frac{6\phi}{d_{32}} \qquad [7]$$

Furthermore, free surface flows are characterized by Froude number, Fr.

The most useful dimensionless number is the Modified Froude Number (N_{Fr}); which characterizes the fluid flows generated by gas injection in B.O.F, A.O.D and C.L.U. Hence, the dynamic similarity is defined for the present model by equation:

$$N_{Fr} = \frac{\rho_g}{\rho_l} \frac{U^2_{g.nom}}{gd} \quad [8]$$

Where,

ρ_g represents the gas density (Kg / m^3)

ρ_l is the liquid phase density (Kg / m^3)

$U_{g.nom}$ is the nominal velocity at the nozzle (m / s)

d is the nozzle diameter (m)

g is the gravitational acceleration

Numerous investigators took into account geometric and dynamic similarities to correlate physically model to the prototype. Both criterions are paramount in the framework of the current work.

(c1) Froude Number and its applications

Froude number and its modifications have been used so much with keen interest by several researchers in their investigation on water modeling techniques for correlating the model and the real system.

G.Akdogan and R.H.Eric [38], M.S.Lee and H.Y.Sohn [37] used the Froude number to simplify the correlation of the hold up in their investigation of physical modeling of emulsions. In this case, the Froude number represents the combined effects of the gas flow rate, injector diameter, and height of the heavy phase.

Numerous investigators [43-44] used the modified Froude number in their similarity considerations for the calculation of the gas injection rate in the model of combined blown steelmaking.S.Kim and Fruehan [44] defined the modified Froude number as the ratio of the kinetic energy of the gas injected through a tuyere to the buoyancy energy

of the gas. Then, the Froude number was considered as the similarity criteria to correlate the gas flow rate between full-scale model and real system.

$$\left(N_{Fr}\right)_{System} = \left(N_{Fr}\right)_{Model} \quad [9]$$

Fabritius, et al [24] pointed out the importance of the Modified Froude number for describing gravity, buoyancy and inertial force in A.O.D. bath.

From literature survey, it was clear that the Froude number is the most important dimensionless number used in dynamic similarity for correlating model to the prototype in systems using gas injection. Hence, the following relationship may be applied to the current model.

$$\left(N_{Fr}\right)_{CLU} = \left(N_{Fr}\right)_{Model} \quad [10]$$

(C2) Determination of the modified Froude number for the current work

The modified Froude Number was used to relate the model to the prototype. A number of investigations have been performed on 0.2 scale model of the commercial CLU [39, 45, and 36].

Since the tank is open to the atmosphere and the densities of the simulated phases (slag and metal) are known; the pressure exerted by the fluid at the bottom of the tank can be calculated. Taking into account an averaged bath height of 54.5 cm, the pressure is calculated by means of the following hydrostatics relationship;

$$P_2 = P_1 + \rho_l * g * H_L \quad [11]$$

Where P_1 is the atmospheric pressure, P_2 is the pressure exerted by the liquids, H_L is the height of the liquid phases and g is the acceleration due to gravity. Hence,

P_2=1.013+ [(1000*0.9+860*0.1)*9.81*0.54]/100000

P_2=1.065 Bar

The density of compressed air used in the model can be estimated since the pressure at bottom is known through the relationship:

$$\rho_{air-model} = 1.29 * \left(\frac{P_2}{P_1}\right) * \frac{273}{T}$$

$$= 1.29 * \left(\frac{1.065}{1.013}\right) * \frac{273}{293}$$

$$= 1.26 \text{ Kg.m}^{-3}$$

Considering the averaged gas flow rate of 0.0145 m^3/s under CLU model operating conditions, the gas flow rate at the nozzle tip is given by the following expression;

$$Q_{Actual} = 0.0145\left(\frac{1.013}{1.065}\right)\left(\frac{293}{273}\right)$$

$$= 0.0148 \text{ m}^3/\text{s}$$

The nominal gas velocity can be calculated through the following relationship;

$$U_{nom} = \frac{4*Q}{n\pi*d^2} \qquad [13]$$

Where, d is nozzle diameter $= 6\times10^{-3} m$ and n is number of nozzle

$$= \frac{4 * 0.0148}{5 * 3.14 * \left(6 * 10^{-3}\right)^2}$$

$$= 104.8 \text{ m/s}$$

Finally, the modified Froude number for the model is calculated from equation 8 as follows;

$$N_{Fr} = \frac{1.26}{986}\left(\frac{104.8^2}{9.81 * 6 * 10^{-3}}\right)$$

$$= 238$$

The efficiency of the blowing gas is a primary requirement in the homogenization of the bath. The metallurgical campaign is such that the less the carbon is in the molten steel, the longer the gas injection will last. To achieve this purpose, there is the need of fluctuating the gas flow rate as well as the modified Froude number (See Table 2). The modified Froude number is basically a function of the gas flow rate as can be seen in Figure2.

Table2: Ranges of modified Froude Number

MODEL	RANGES
Current work	72 – 410
Admire and Nyoka[45,22]	Calculated averaged value 252
Akdogan and Eric[39]	4000 – 10000
Vanyukov Process[23]	0.273 – 2.14

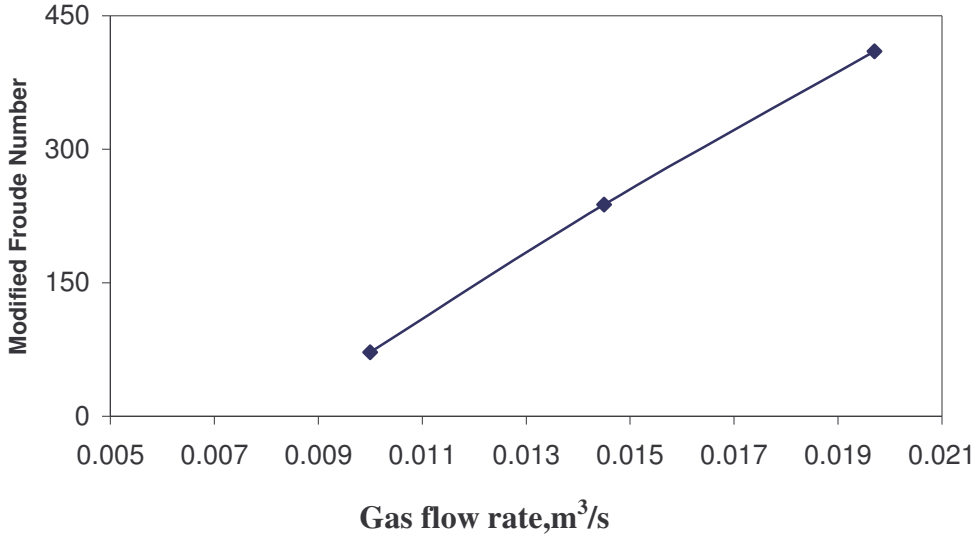

Figure2: Modified Froude Number as a function of the gas flow rate

2.4.2 Types of process model

In modeling of a process, it is necessary to have in mind the difference between a simulation model and design model [46].A simulation model is written or used to simulate existing plant or equipment. Outputs are calculated exactly as an existing plant. The design model is needed where no equipment exists and a plant design is required for a particular output. The current work focuses on the simulation model of dispersion in the 100 ton CLU reactor operated by Columbus stainless steel.

.

Table 3: Comparison between parameters used in the prototype and the model**.**

Parameter	Prototype	Model
Liquid 1	Molten steel	Water
Liquid 2	Molten slag	Paraffin
Purging gas	Steam/Argon/nitrogen/Oxygen	Air
Vessel material	Steel and refractories	Clear 6mmPVC
Nozzle diameter	30mm	6mm
Number of nozzles	5	5
Bath height	2.2;2.75;3.29m	0.435;0.55;0.658m
Purging gas flow rate	0.93 - 1.77Nm^3/s	0.01-0.019m^3/s
Modified Froude number	72 - 410	72 - 410
Kinematics viscosity	10^{-3}kg/m.s	10^{-3}kg/m.s
Density	7200kg/m^3	1000kg/m^3
Temperature	1700^0 C	20^oC

In Table 3 are displayed relevant parameters and operating variables used in the modeling of the CLU reactor.

2.4.3 Construction of mathematical models

2.4.3.1 Definition of mathematical models

A model is basically a representation of a process [47].A mathematical model takes the form of a set of equations describing a number of variables. The mathematical model used in the present work and in most investigations previously carried out on water modeling techniques, expresses physical phenomenon like emulsion, mixing time, mass transfer and size distribution of droplets. The mathematical equations are useful for further industrial applications and also to better correlate relevant parameters [38, 37, and 31].There are four stages in mathematical models [48].

a) Setting the objective

The purpose of this step is to make a decision on systems to model. In the current work, the system to model is the bath smelting of the commercial 100-ton C.L.U. converter.

b) Choosing the equations

This stage is related to the collection of mathematical equations representing the system. For them to make sense, these equations must describe sufficiently the system in order to involve all the relevant factors. Dimensional analysis was used as a tool to achieve this goal in the present work. The form of the equations describing the dispersion phenomena could be linear or nonlinear according to the experimental results.

c) Formulation of the model

After getting the form of all equations describing the model, the aim of this step is to solve these in order to give the answer required by the model. The application of Buckingham pi-theorem is useful at this step. The use of particular software such as Datafit, Matlab and Surfer.32 was recommended in order to build up the model.

d) Fitting the model

The purpose of fitting is to define clearly the general trend that matches experimental data. Such trend may be found through either linear or nonlinear regression.

2.4.3.2 Dimensional analysis

Marko Zlokarnik [49] defined dimensional analysis as a tool that enables a faster elaboration of a dimensionless set displaying experimental parameters. As such, dimensional analysis is a useful technique in representing the overall effect of complex phenomena encountered in pyrometallurgical vessels.

The purpose in the application of dimensional analysis to the CLU model, is to simply define the overall effect of the phenomenon studied (dispersed phase, mixing time or mass transfer rate) through mathematical expressions that correlate physical variables believed to be of key importance [50].

There are two real problems in dealing with dimensional analysis. The first is the construction of a complete list of relevant parameters that describe the process. The second is the determination of the process characteristics and the establishment of real operational numbers in case of large-scale factors.

Dimensional analysis was utilized by various modelers to outline the effects of dispersion, mass transfer, heat, fluid flow, and so on.

Lee and Sohn [37] used dimensional analysis to correlate the hold-up with the operating conditions and the sampling locations. K.Iyer and Sohn [51] performed dimensional analysis to correlate the energy of the lighter liquid to the operating parameters. By the way of dimensional analysis, Buckingham pi-theorem was applied in order to get relevant dimensionless groups after parameters involved in the process were defined.

S.Ghorai, *et al* [50] used dimensional analysis in their modeling in order to define the overall effect of mass transfer through simple mathematical expression.

Previous investigators [38, 37] applied dimensional analysis to correlate the dispersed phase to the operating conditions.Lin and Guthrie [5] used dimensional analysis to express the volume of lower liquid carried up into the emulsion per bubble.

Buckingham pi-theorem

"The number of dimensionless groups in a complete set is the difference between the total number of variables and the rank of the dimensional matrix." The maximum number of variables in the original set that are not part of a dimensionless group constitutes the rank of the dimensional matrix.

The dimensional analysis has been used fruitfully in the field regarding mixer design and scale-up [47].Mathematically [52], Buckingham pi-theorem can be formulated as follows:

"Assuming that the equation f ($\alpha, \beta, \gamma, \delta$) =0 is to be a complete equation, the solution has the form

g ($\pi_1, \pi_2, \ldots \pi_n$) = 0,

Where the π are the n-m independent products of the arguments $\alpha, \beta, \gamma, \delta, \ldots$ which are dimensionless in the fundamental units.

.

2.4.3.3 Verification of Model –Prototype tolerance

In the scope of the current work, tolerances were examined in terms of standard error of the estimate and R-squared. For the model to best fit, the following condition must be achieved $0 < R^2 \leq 1$.

2. 4.3.4 Overall correlation of the dispersed phase

From literature survey, the variation of the dispersed slag phase holdup in the water plume or in the bath was correlated to the dimensionless operating conditions and to Froude Number or its modifications.

For Akdogan and Eric [38], the overall correlation of the dispersed phase was found to be an expression of the following dimensionless parameters; axial and radial distances, Modified Froude Number and the bath height. The following equation was suggested as the overall distribution of the dispersed slag phase holdup in a one seventh CLU model;

$$\phi(z.r) = \phi_{Centerline}\left[1-\left(\frac{r}{H_w}\right)^2\right]^a + \sin\left[b\left(\frac{r}{H_w}\right)\right] \qquad [14]$$

Where:

$$\phi_{centerline} = 0.22\left[(Nfr)^{0.12}\left(\frac{H_o}{H_w}\right)^{0.74}\left[1-\left(\frac{z}{H_w}\right)^2\right]^{0.483}\right]^{1.02} \qquad [15]$$

Where,

$\phi_{centerline}$ is the dispersed phase hold-up along the centerline

N_{Fr} is the modified Froude number

H_o is the height of the organic phase

H_w is the height of the water

r is the radial distance

z is the axial distance from the original interface

$$a = 0.00062\left[\left(\frac{z}{H_w}\right)^{0.9264}(Nfr)^{0.3278}\left[\frac{H_o}{H_w}\right]^{-1.8219}\right]^{0.7262} \quad [16]$$

$$b = 0.17\left(\frac{z}{H_w}\right)^{0.3523} \quad [17]$$

On the other hand, Lee and Sohn [37] correlated the dispersed phase to the operating conditions such as injector diameter, axial and radial distance, bath height and the Froude Number. Then, they suggested the overall correlation of the dispersed phase holdup as follows:

$$\phi(z,r) = \phi_{centerline} \times \exp\left[-0.693\left(\frac{r}{r_{0.5}}\right)^2\right] \quad [18]$$

Where, $\phi_{(z,r)}$ is the dispersed phase at the position (z,r), r is the radial position and $r_{0.5}$ is the radial distance where the dispersed phase is half the maximum value at the centerline.

The survey of literature emphasized that the inverse emulsion occurs in bottom blown converter when the lighter phase (slag) is smaller in volume than the continuous phase (steel).The modified Froude Number was considered as the dynamic criterion to correlate CLU model and CLU prototype. The dimensional analysis is a simple approach in modeling the dispersed phase in bath smelting.

3 EXPERIMENTAL PROCEDURE

3.1 Experimental technique

The experimental set-up comprised of a cylindrical clear PVC tank, which is a one – fifth model of the commercial CLU converter and a flow meter for air flow regulation as shown in Figure 3.5. For simulations purposes; water and paraffin were used respectively. Physical properties of simulated phases are given in Table 4.

Tapped water (simulated molten steel) and paraffin oil (simulated slag) were filled in to the tank at 90 % and 10 % by volume respectively. Water and paraffin heights are given in Table 6. The height of water was directly measured by means of the ruler fixed along the CLU model. The frequency of filling was such that water came first as dense phase and then paraffin. The reason why was to avoid deformation of the original interface before gas injection. During experiments the air flow rate varied from 0.01 m^3/s and 0.019 m^3/s. Experiments were run by injecting compressed air into the bath through fives nozzles located at the bottom the right side (See Figure 3.4). The axial and radial position from where the samples were taken, were recorded together with the gas flow rate and the heights of water and paraffin before gas injection.

After a half an hour injection period, a sample emulsion was collected rapidly at a particular position by means of specially made syringe fixed firmly by the clamps. Then, the sample emulsion was transferred to the measuring cylinders. Owing to the fact that the measuring cylinders were motionless, the separation of phases took place as droplets oil coalesced upwards; due to the low density of the lighter phase.

Oil drops gathered on top of the dense simulated metal (water) and the demarcated original interface appeared after complete phase separation.

After a half an hour, the volumes of water and oil were recorded. Samples were taken from the right-axis (directly above the nozzles) of the tank as well as the left axis (See Figure 3.3).Sample emulsions were taken eight times at a time interval of three minutes and the averaged value of the dispersed slag phase was calculated by means of the relation:

$$Dph = \frac{V_O}{V_O + V_W} \qquad [19]$$

Where, V_o is the volume of oil, V_w is the volume of water and Dph is the dispersed phase hold up.

Appendix A up to appendix D summarizes details on the dispersed phase for each sample emulsion collected as well as the corresponding average. All investigations were run at room temperature. The experimental work focused essentially on two key parameters; the axial measurements and the radial measurements.

Table 4: Physical properties of liquid phases at 20 ° C

Liquid	Density (Kg/m^3)	Interfacial tension $(dyne/cm)$	Viscosity (cP)
Water	1000	1	
Paraffin- oil	865	50	55

3.2 Radial measurements of the dispersed slag phase

Samples along the radial axis were taken in the plume region from the center and in the vicinity of the wall side as shown in Figure 3.2. The defined radial distances were 0; 9.7 and 19 cm respectively covering nearly the entire bath. Sample statistics were as follows,

- 6×3 along the radial axis located exactly at the origin.
- 6×4 along the radial axis placed at 90 degrees from the horizontal axis.
- 6×4 along the radial axis located at 135 degrees
- 6×4 along the radial axis situated at 45 degrees.

Thus all sampling positions yield a total of 90 samples**.** During axial and radial measurements, the gas flow rate and the bath height were kept constants.

Table5: The vertical coordinates of the samples

SAMPLE	WATER HEIGHT (4 0 *Cm*)	AXIAL DISTANCE Z(*Cm*)
S1	35	5
S2	30	10
S3	25	15
S4	20	20
S5	15	25
S6	10	30

There are 15 radial positions at each axial axis. The axis AB in Figure 3.3 represents the horizontal centerline, which separates the right side from the left. The distribution of the dispersed along the axial centerline has been investigated by taking into account all the sampling positions along the axis AB.

3.3 Axial measurements of the dispersed phase

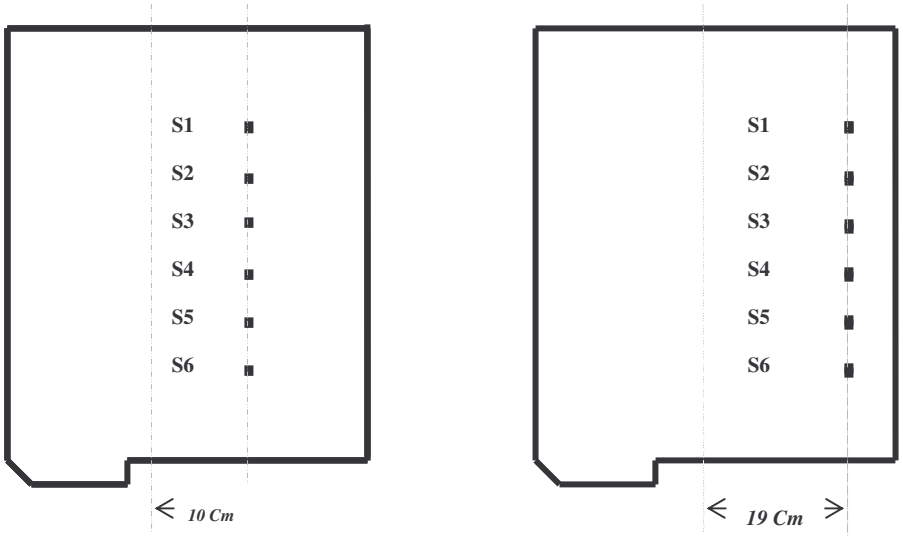

a) ***Axial sampling positions on the right side***

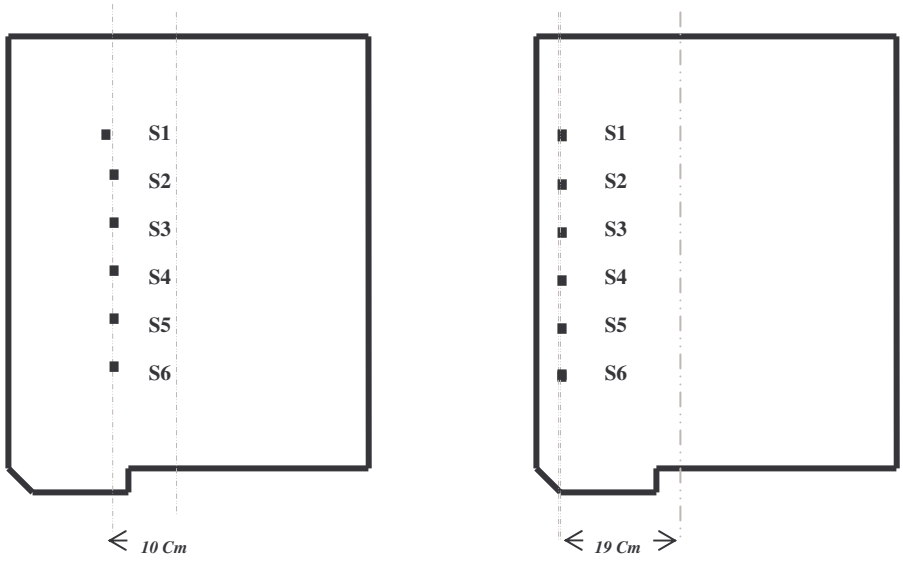

b) ***Axial sampling positions on the left side***

Figure 3.1: Side view of axial sampling positions

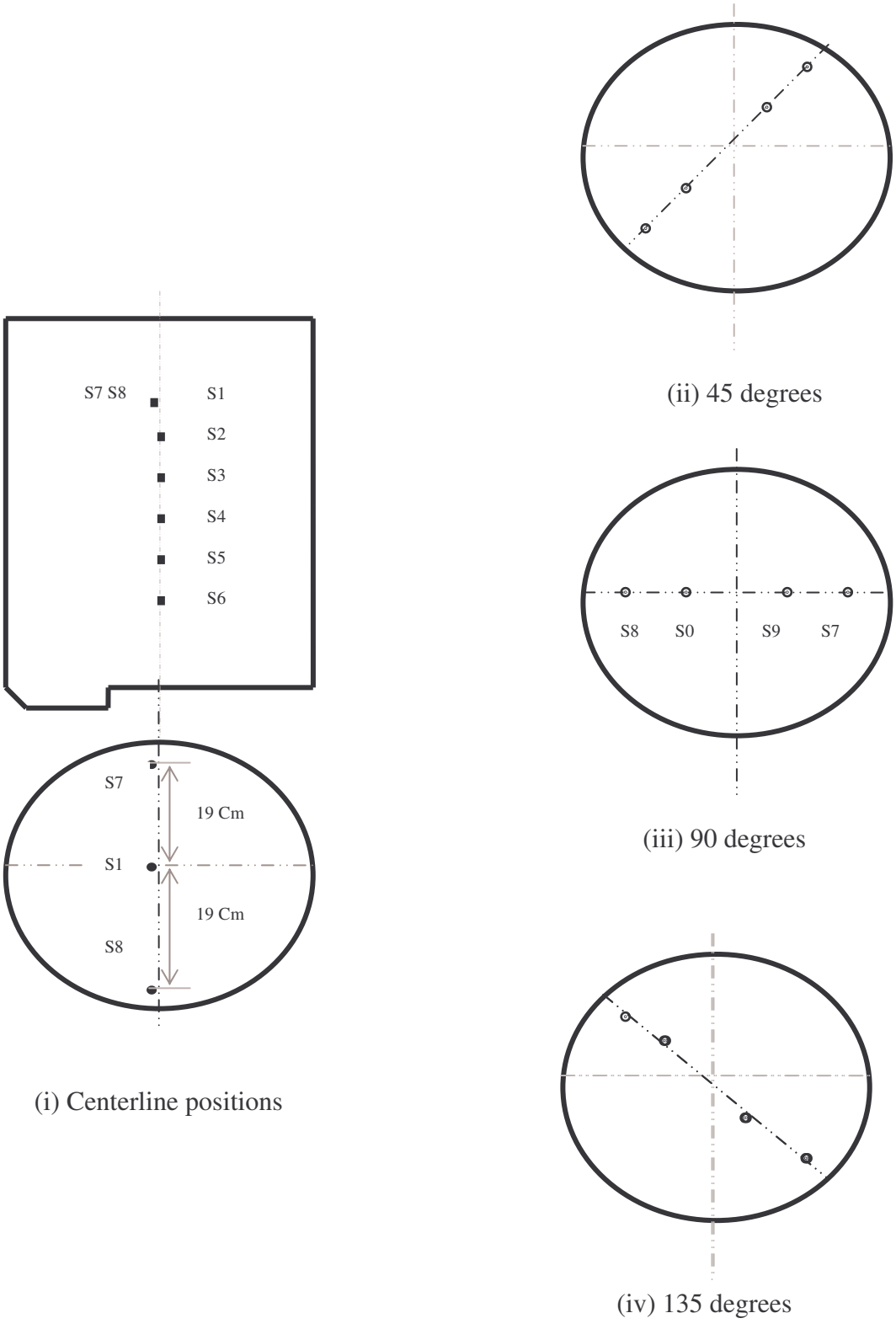

Figure 3.2: Top view of radial sampling positions

The measurements along the vertical axis were carried out on different sides of the vessel as shown Figures 3.1 and 3.2 as follows;

- At the central section, samples were collected in three axes whose distance from the axial centerline was 19 cm. The averaged value of the dispersed phase was calculated.
- Samples were taken also along the vertical axis located at 9.7 Cm from the axial centerline. Six axes were considered in three different sections which make with the vertical axis an angle of 45, 90,135 degrees respectively. The averaged value of the dispersed phase was calculated for both sides of the bath (left and right) at the particular sector.
- Sampling measurement was extended to the section close to the wall side 19 Cm away from the axial centerline; for assessing the impact of the wall side on the dispersed phase. Likewise, six axes were considered as can be seen in Figure 3.1. Each side of the bath was characterized by a specific behaviour of the fluid flow depending on the turbulence intensity, interfacial tension between simulated slag and metal. In Table 5, the values of the axial distance from the original interface are displayed. The sampling process started 5 cm away from the original interface downwards. As the axial distance decreased, the water height decreased as well.

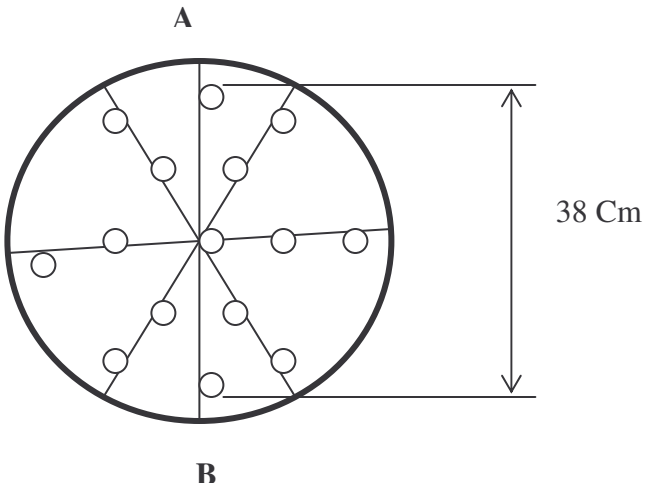

Figure3.3: Top view of sampling positions

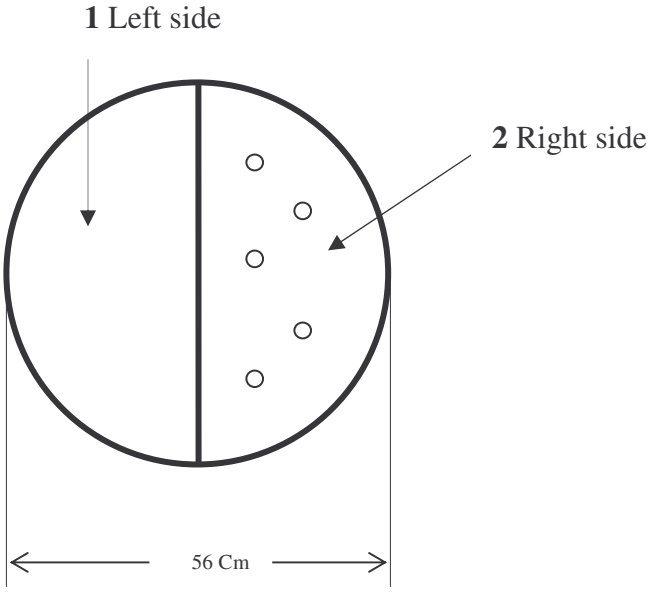

Figure3.4: Top view of nozzles position

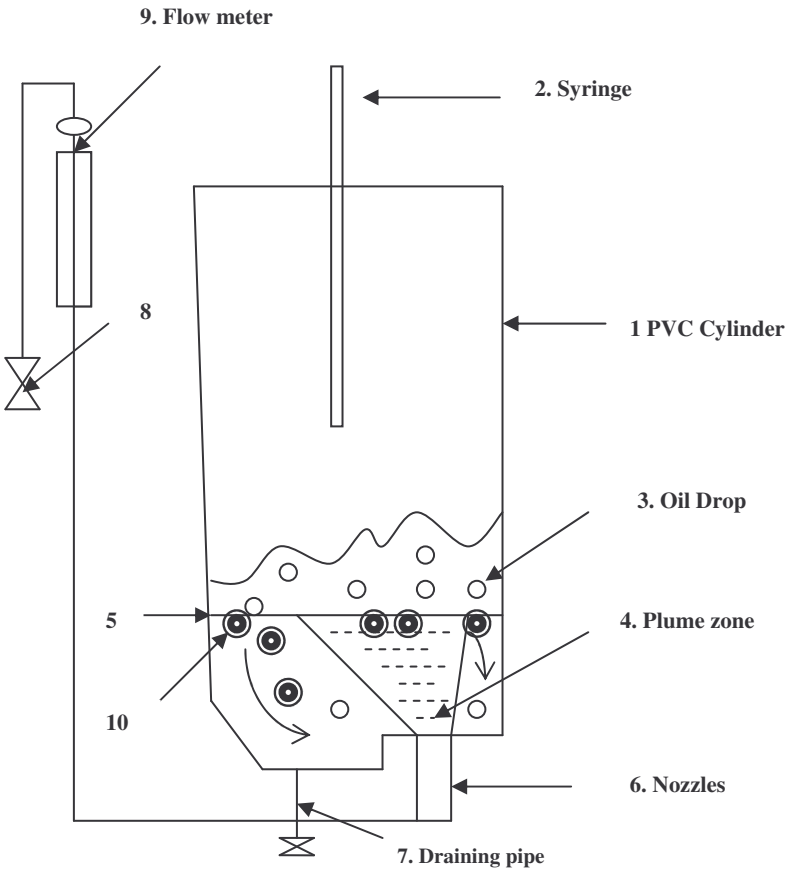

Figure 3.5: The Schematic representation of the experimental set-up

5-Original interface

7-Draining pipe

8-compressed air-valve

9-Air flow meter

10-water Drop

3.4 Bath height optimization

The bath was divided in to four sections located at the positions 0; 90; 45 and 135 degrees respectively as shown in Figures 3.1 and 3.2. And at each section, samples were collected radially and axially.

The first stage during the experimental work focused mainly on the optimization of the bath height in order to conduct investigations on the dispersed slag phase. Tests were carried out at various bath heights. The values of the dispersed phase correlate with the operating variables at the bath height of 43.5 cm as shown in appendix A. In appendix D and E, there is a discrepancy between the gas flow rate and the dispersed phase values. Hence, the results revealed that the bath height was optimum when it was lower (43.5 cm).Then; most of the results presented in the current work were related to the bath height optimum.

Table 6: Bath height and volume total at 10 % volume slag

Water Height (m)	Paraffin Height (m)	Bath Height (m)	Water Volume (m^3)	Paraffin Volume (m^3)	Bath Volume (m^3)
0.40	0.035	0.435	0.078	0.009	0.087
0.50	0.046	0.546	0.102	0.011	0.113
0.60	0.058	0.658	0.128	0.014	0.142

The CLU converter is composed of a conical shape at the bottom and the cylindrical part. The volume of the bath in the current work was defined as the sum of the volume of water and volume of paraffin. For 10 % by volume of simulated slag, the following relationship may be written,

$$\frac{V_p}{V_w + V_p} = 0.1 \quad \text{..... [20]}$$

Where V_p and V_w represent the volume of paraffin and water respectively.

Table 6 shows the relationship of the volume of paraffin to the volume of water.

As shown in Figure 3.5, the right side characterized the side where nozzles were situated .The water plume was mainly formed in that zone and buoyant forces were also much pronounced. The right side was the starting region of dispersion of oil, characterized by intense turbulent flow. From one position to another, eddies produce visible fluctuations in the flow, velocity and pressure. The left side of the set up was a recirculatory region that was characterized by circulating loop induced by the movement of the water plume.

The experimental work aimed to investigate the dispersion behavior of the slag phase at various operating conditions namely gas flow rate and bath height as a function of axial distance and radial distance, as well as to shed light on the variation of the dispersed phase from the right axis to the left axis.Thereafter, the dispersed phase model was established on the basis of the experimental results and the modified Froude number. Operating conditions selected for the experimental work are summarized in Table 7.

4 RESULTS AND DISCUSSION

Dispersion of oil into the bulk simulated metal (water) is the result of bottom gas injection in to the bath, which causes bubble formation in such a way that bubbles rising entrain a bulk liquid upwards according to the operating conditions and the buoyancy transferred to the liquid in the ascending movement. The deformation of the original interface (Rayleigh and Helmholtz instability) occurs generating a number of liquid drops once the three -phase bubble-water-oil reaches the free surface.

4.1The effect of the gas flow rate on dispersed slag phase hold up

4.1.1The effect of the gas flow rate on the right side

The effect of the gas flow rate on the dispersed slag phase was investigated by maintaining the bath height constant and varying the flow rate between 0.01 m^3/s and 0.019 m^3/s .The operating variables are illustrated in Table 7.Tests on the dispersed slag phase were carried out step by step from the plume zone towards the wall side of the tank. The effect of the gas flow rate on the dispersed phase on the right side is shown in Figures 4.1 to 4.4 on the sections situated at 90 degrees, 45 degrees and 135 degrees.

Table 7: Ranges of operating variables

Variable	Range
Gas flow rate,m^3/s	0.01 – 0.019
Height of water, m	0.40
Height of oil, m	0.035
Bath height, m	0.435
Axial distance, cm	5 - 30
Radial distance, cm	0 – 19

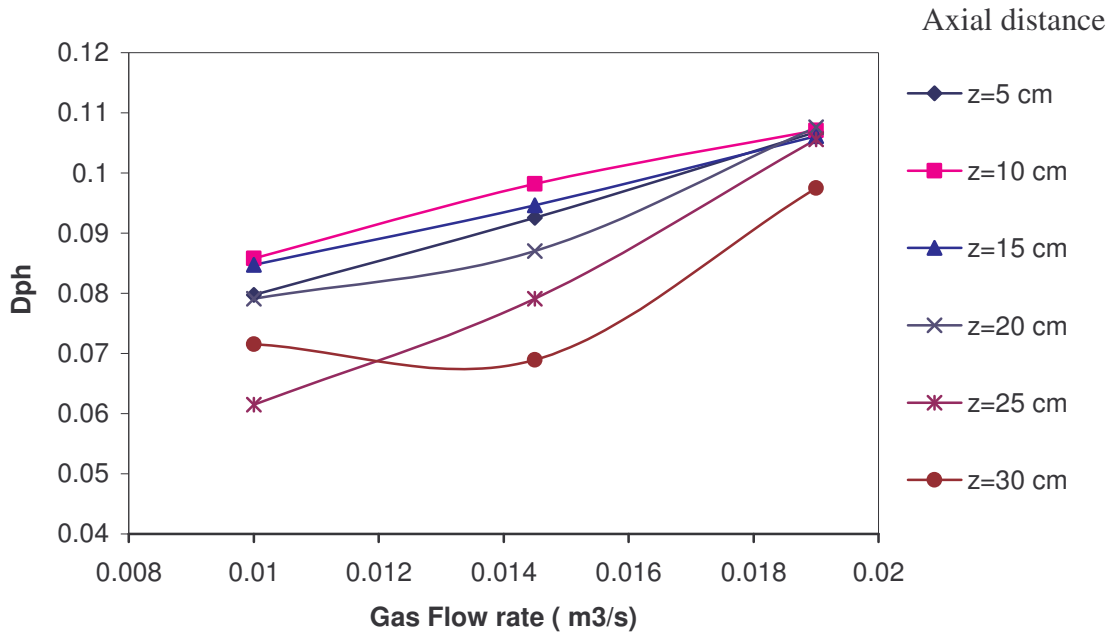

Figure4.1: Variation of the dispersed slag phase with the gas flow rate on the right side (Radial distance=19cm, 90 degrees)

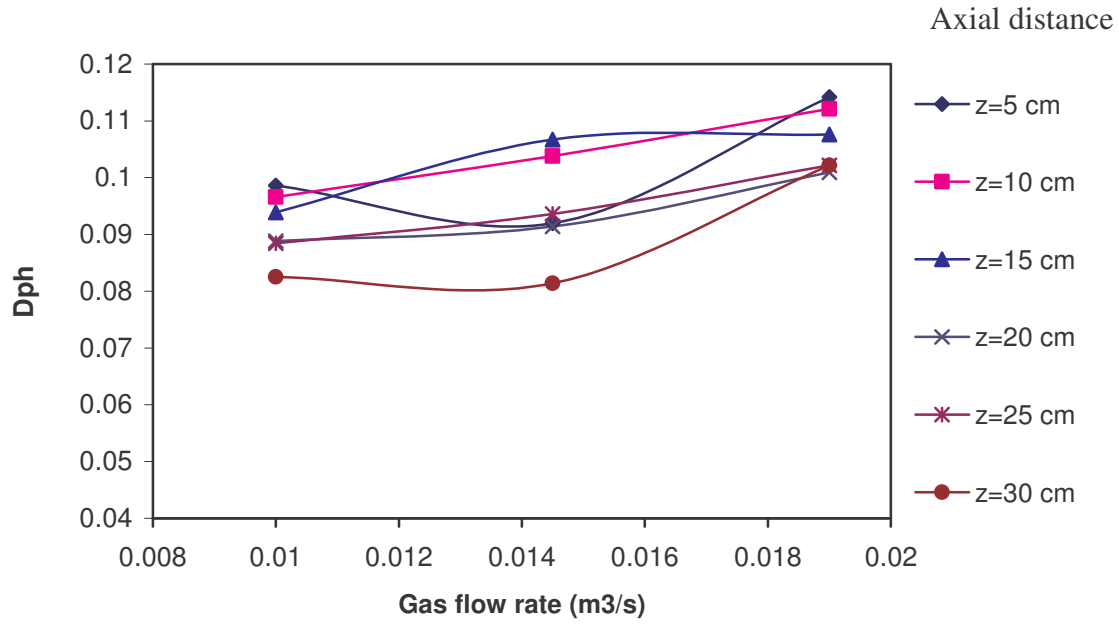

Figure 4.2: Variation of the dispersed slag phase with the air flow rate on the right side (Radial distance =19 cm, 45 degrees)

As depicted in Figures 4.1 to 4.4, the dispersed slag phase increased with an increase in the flow rate in the plume zone at the radial distance of 9.7 cm from the center and in the recirculation towards the wall side at the radial distance of 19 cm. Such effect of the flow rate was observed at various axial distances from the top of the bath downwards**.** This result might be explained by the intense turbulence in the water plume and by the disintegration of oil drops as the gas flow rate increased.

In the plume zone, oil droplets were subjected to stronger buoyancy to such an extent that their surface tensions as well as the gravity are weaker. Then, the circulation of oil droplets into the bath became faster and very turbulent at the radial distance of 9.7 cm. The plume zone was more emulsified than the recirculation zone as can be observed from figures 4.1 and 4.4. An increase in the gas flow rate involved an increase in droplet number and a decrease in droplet diameter.

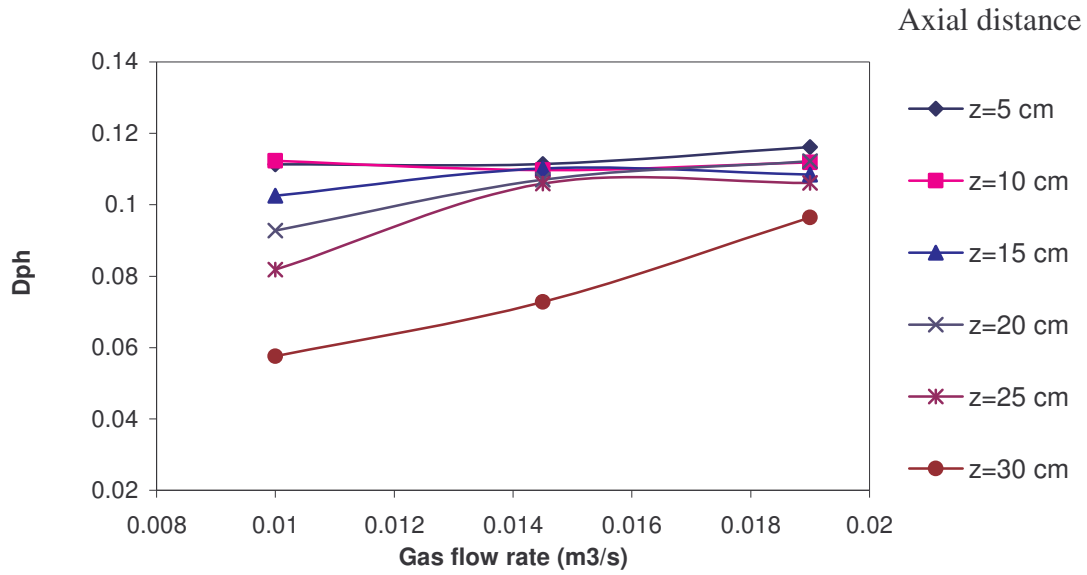

Figure 4.3: Variation of the dispersed slag phase with the air flow rate on the right side (Radial distance = 9.7 cm, 90 degrees)

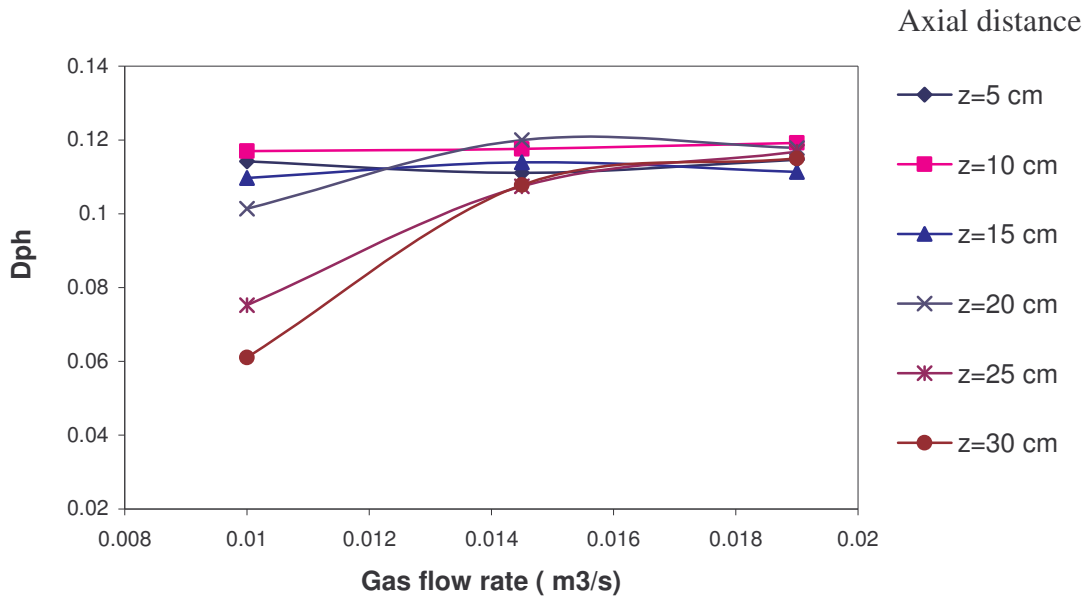

Figure 4.4: Variation of the dispersed slag phase with the gas flow rate on the right side (radial distance = 9.7 cm, 135 degrees)

The number of oil droplets formed in bath depends on the position (axial and radial) as well as on the interaction of dynamic forces namely surface tension, inertia force, buoyancy and gravity. The intensity of those forces depend naturally on the turbulence effect, the nature of fluid movement (either accelerated or not) and the position. This result showed good agreement with the finding of Phelan and Brooks [23] .They observed that coalesced droplets become unstable at higher gas flow rates and break into smaller droplets; as a result decreasing the mean droplet diameter.

4.1.2 The effect of the gas flow rate on the left side

The dispersed slag phase increased also with the stirring gas rate on the left side. Such observations were made in the region situated between the axial distance z=20 cm and z=30 cm as shown in Figures 4.5, 4.6 and 4.7. Dead zones were observed at the free surface of the bath on the left side, especially at relatively lower gas flow rate, due to the weakened turbulence effect. A loop circulation was the main feature of flow patterns on that side .Oil phase emulsified easily into the water plume as the gas velocity increased at the nozzle tip.

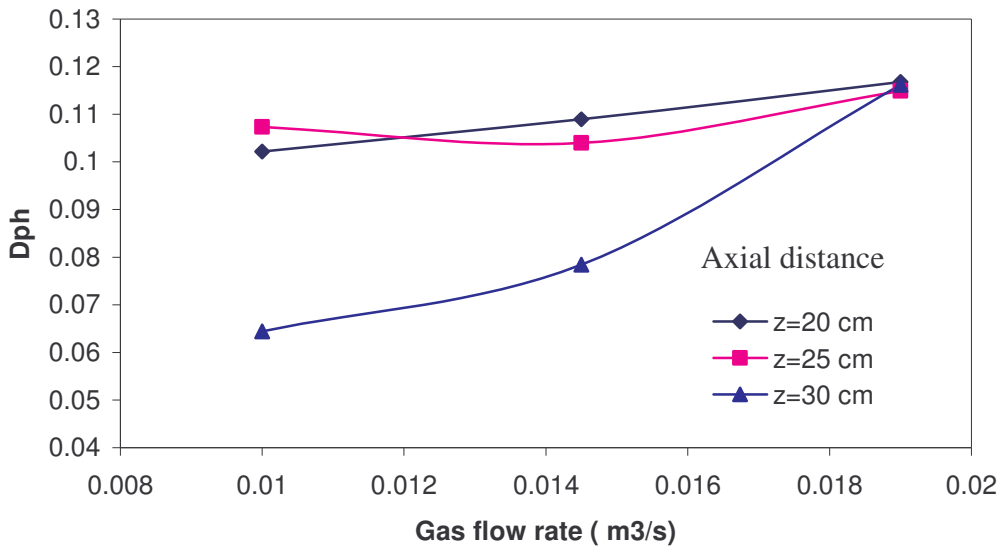

Figure 4.5: variation of the dispersed slag phase with the gas flow rate on the left side. (Radial distance = 19 cm, 45 degrees)

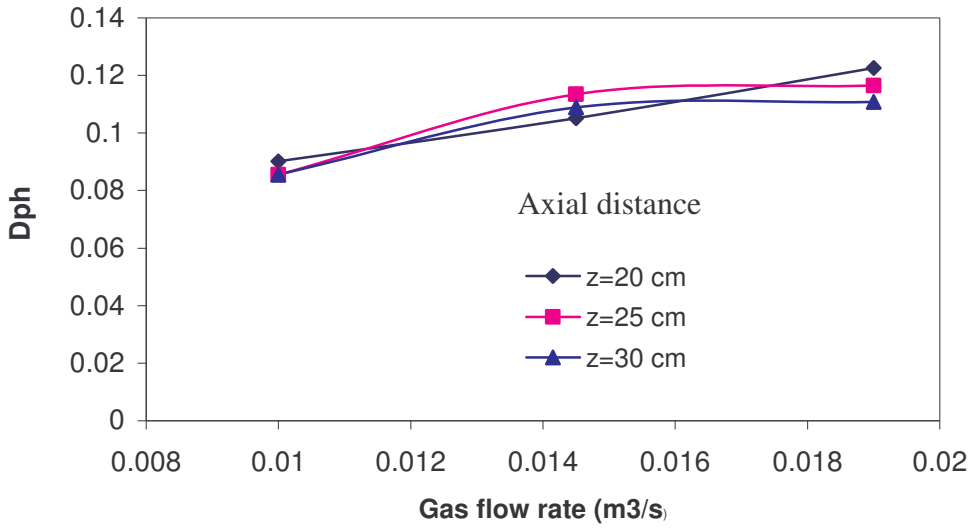

Figure 4.6: Variation of the dispersed slag with the gas flow rate on the left side (Radial distance = 9.7 cm, 45 degrees)

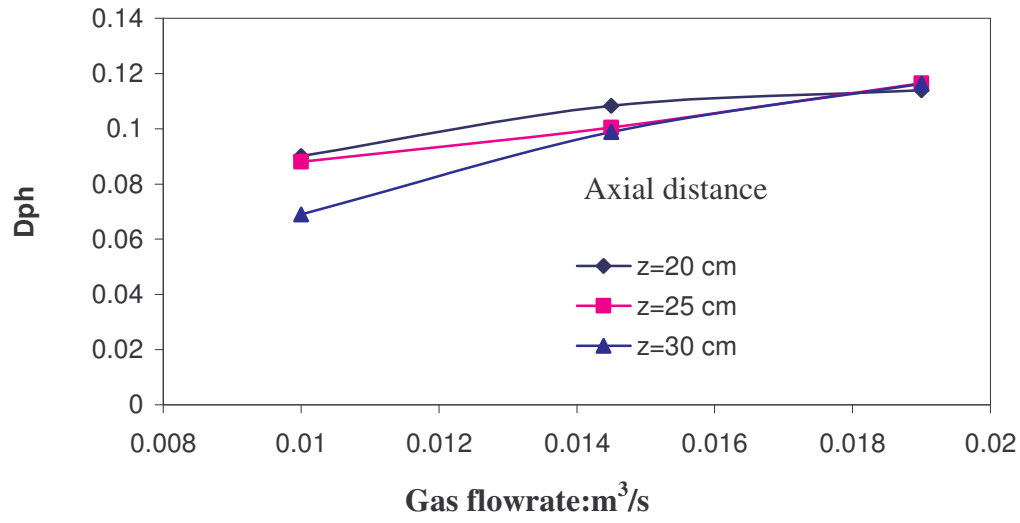

Figure 4.7: Variation of the dispersed slag with the gas flow rate on the left side (Radial distance = 9.7 cm, 135 degrees)

Previous investigators agreed on the fact that increasing gas flow rate enhances the rate of emulsion in the bath smelting. Most of them were focused on the water plume zone [38, 37, and 31]. Akdogan and Eric's [39] investigation emphasized that increasing the

gas injection increased the water plume cone; resulting in enlarged plume radius at the surface. As a result, the plume volume was increased in the bath and the circulation of oil drop was enhanced in the water. The air flow rates ranged between 0.00599 to 0.01465 m^3/s. As asserted in recent investigations [22], the difference observed in the results of Akdogan and Eric with the current work, was attributed to decreasing turbulent variables in 0.2 scale CLU model as a result of stirring energy dissipation. The intense emulsion observed at higher gas flow rate was attributed to the effect of instabilities, due to fragmented body forces on the emulsified oil layer [53].

Admire's [22] investigations showed that the presence of circulation cells and dead volumes impacted negatively on the left side of the vessel. As a result, the dispersion of oil slowed down in that region due to the higher surface tension between the simulated phases.

S.J.Buckler *et al.* [54] carried out investigations aimed at the measurement of the total interfacial area during submerged gas injection into a liquid bath. They found out that the total interfacial area increased with increasing the gas flow rate. Thus, increasing the interfacial area implied an increase in the reaction rate. In the current research, the effect of the flow rate was extended to the entire bath.

Increasing the air flow rate in the CLU bath improved both turbulence and mixing. Such effects lead to the greater number of slag drops and bubbles. Accordingly, the more oil drops are, the greater the volumes of dispersed phase will be. Thus, an increase in the flow rate makes the jet continuous favouring the multiplication of bubbles and reduces the surface tension between the fluids.

The increasing dispersed phase found when the gas flow rate increased, is in great part the reason that explains satisfactorily the enhanced mass transfer in the CLU reactor at higher gas flow rate. It goes without saying a word that the modified

Froude Number is directly proportional to the gas flow rate such that analogues trends were observable as graphed in Figure 4.8.

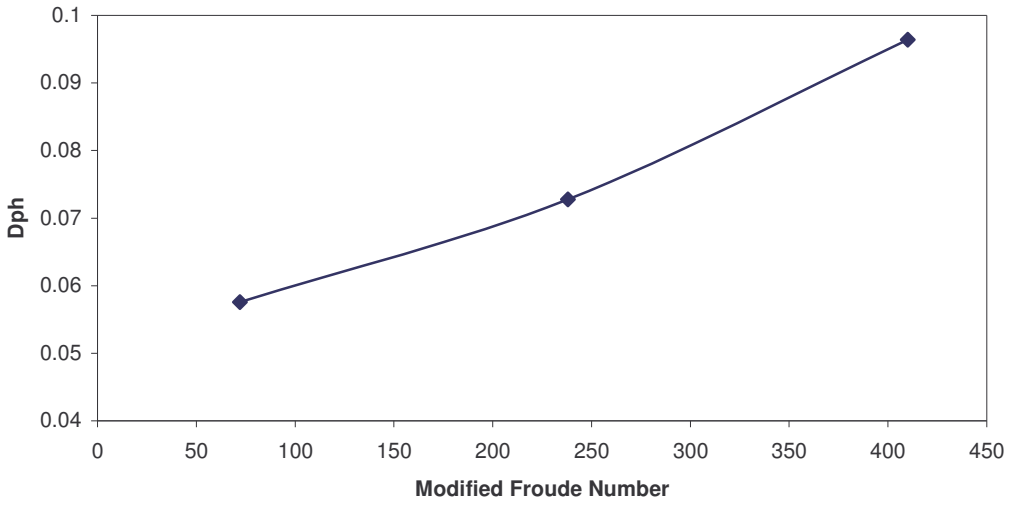

Figure 4.8: Variation of the dispersed slag phase with the modified Froude Number

4.2 Specific energy input

The total stirring energy supplied to the bath is the sum of the buoyancy energy (E_b) supplied by the gas bubbles rising in the liquid and the kinetic energy of the gas in the jet. The buoyancy energy is given by the following relationship [22],

$$E_b = 0.01425QT\log\left(1+\frac{H}{1033.9}\right)\frac{1}{W} \qquad [21]$$

Where

Q is the gas flow rate $(NL/\min)$

T is the temperature (K),

H is the bath height (cm),

W is the weight of the water (ton),

E_b is the stirring energy due to buoyancy (W/ton)

The kinetic energy transferred to the bath is given by [22],

$$E_k = \frac{\rho_g Q^3}{2WA^2} \qquad [22]$$

Where

E_k is the stirring energy due to kinetic energy of the gas in the jet (W/ton)

A is the cross-sectional area of the nozzle (m^2)

ρ_g is the density of the gas (Kg/m^3)

Equations [21] and [22] indicate that both the buoyancy and kinetic energy of the dispersed slag phase are directly proportional to the gas flow rate. Tanaka and Guthrie [7] argued that a higher rising plume velocity will result in a higher reverse flow around the rim of the upwelling fluid. This implies that the greater the rate of energy input into the rising plume of the lower phase liquid ,the greater will be the reversing downwards flow and the greater will be the size of the upper phase particles that can be entrained. Krishna and Mehrothra [55] on the other hand, asserted that the effectiveness of mixing depends on the gradient of convective velocities of the liquid and eddy diffusion. These two parameters are generated by breakdown of larger clumps of liquid into smaller ones. The progressive disintegration of eddies depends on the mode of stirring of the liquid bath and on the quantity of input energy.

4.3 The axial distribution of the dispersed slag phase

The axial dispersed slag phase was estimated by keeping the bath height at 43.5 cm and the gas flow rate constant ($0.01 m^3/s$).

Results of the axial distribution of the dispersed phase are plotted in Figure 4.9 to 4.12. The vertical distance starts five centimeters below the original interface and

extends to the range $z = 30$ Cm. As can be observed the dispersed slag phase decreased with the axial distance from the original interface in distinct sections of the bath. This trend might be explained in terms of bubbles and eddy frequency as well as by the kinetic energy of the liquid phases. The upper zone was the most turbulent and wavier than the bottom side, in which a few oil drops circulate by lack of bubbles and eddy. Much of the kinetic energy of the fluid is associated with the large size eddies.

Other investigators found out that the decrease of the dispersed slag phase with the vertical distance was due to the loss of kinetic energy by collision and viscous friction [37]. Researches on the axial liquid velocity and axial gas in submerged converters were undertaken [56, 57, and 62]. By using electrical resistivity probes and propeller flowmeter, it was found that both quantities decreased as one moved away from the nozzle. Their observation might explain the ascending movement of the water plumes rather the anticlockwise motion of the dispersed oil phase.

Turkdogan [10] investigations identified the liquid phase behavior in submerged lance blown converter in two distinct regions;

1) The upper level ($z = 15$ cm till $z = 5$ cm) that was characterized by prevailing gas bubbles in liquid phase.
2) The bottom level ($z = 20$ cm till $z = 30$ cm) where liquid fragments were found in gas phase.

Two physical phenomena could justify the decrease of the dispersed phase with the vertical distance. On the right side; the pumping action of the plume diminished the momentum transferred to the dispersed phase. On the other hand, the presence of dead zones in the upper zone of the bath created apparently a greater dispersion towards the top side in the recirculation zone. In a recent investigation [22], dead volumes in the CLU model were observed at the bottom of the vessel as a result of minimal kinetic energy and bubble formation. That result was in line with the finding of Lee and Sohn [37].They explained the decrease in the dispersed phase by the decrease in the kinetic energy due to collision and viscous friction.

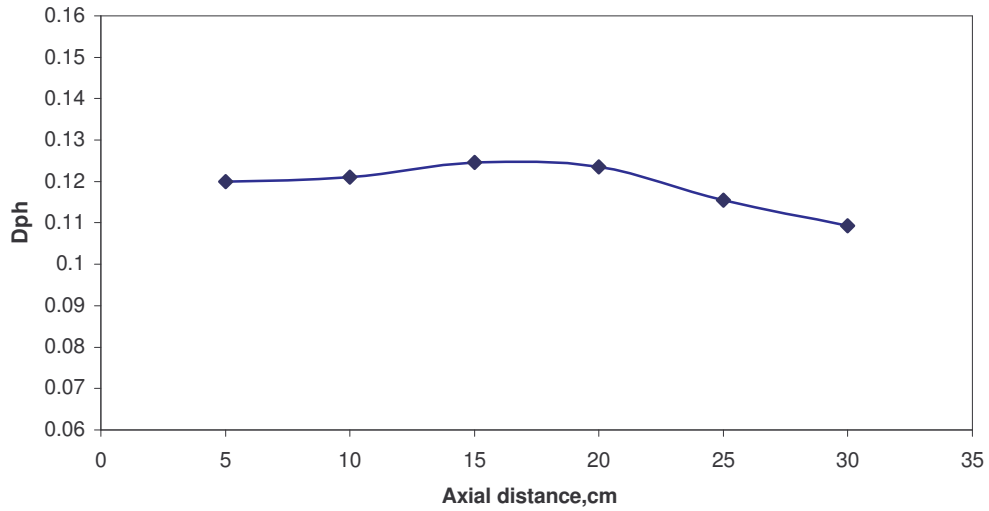

Figure4.9: Variation of the dispersed slag phase holdup with the axial centerline (Gas flow rate: 0.01m^3/s)

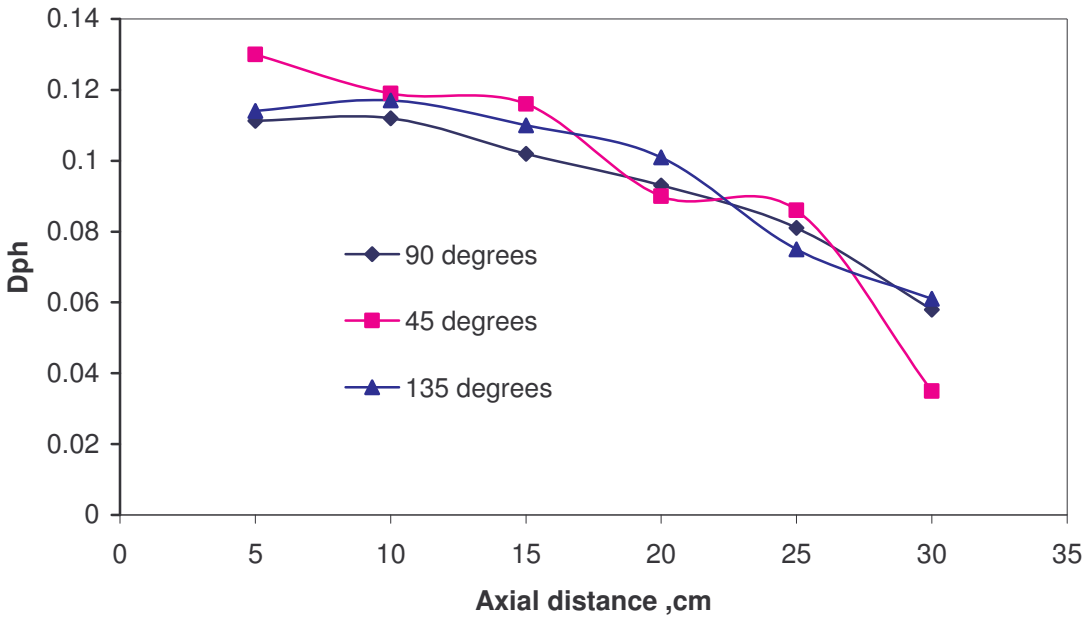

Figure 4.10: Variation of the dispersed phase with the axial centerline at the gas flow rate 0.0145 m^3/s

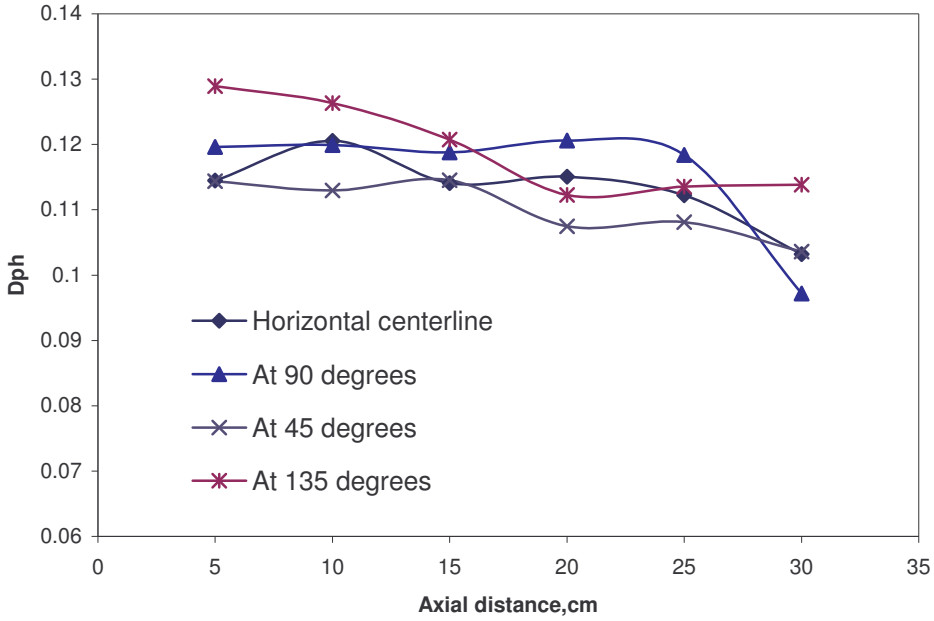

Figure 4.11: Variation of the dispersed slag phase with the axial distance (Gas flow rate = 0.019 m^3/s)

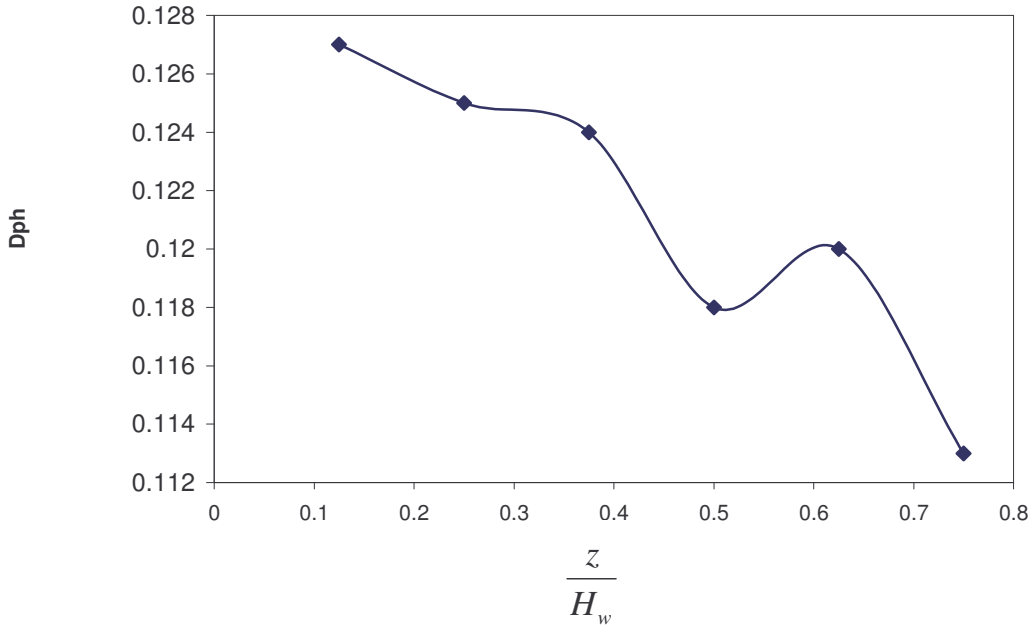

Figure 4.12: Variation of the dispersed slag phase with the dimensionless axial centerline at the gas flowrate:0.019m^3/s

4.4 The radial distribution of the dispersed slag phase

The radial dispersed phase was studied by maintaining all operating conditions constant and varying only the radial distance in the range 0 – 19 cm.

In Figure 4.13 to 4.14, the dispersed phase is plotted against the radial distance at higher flow rate (0.019m^3/s and 0.014 m^3/s).

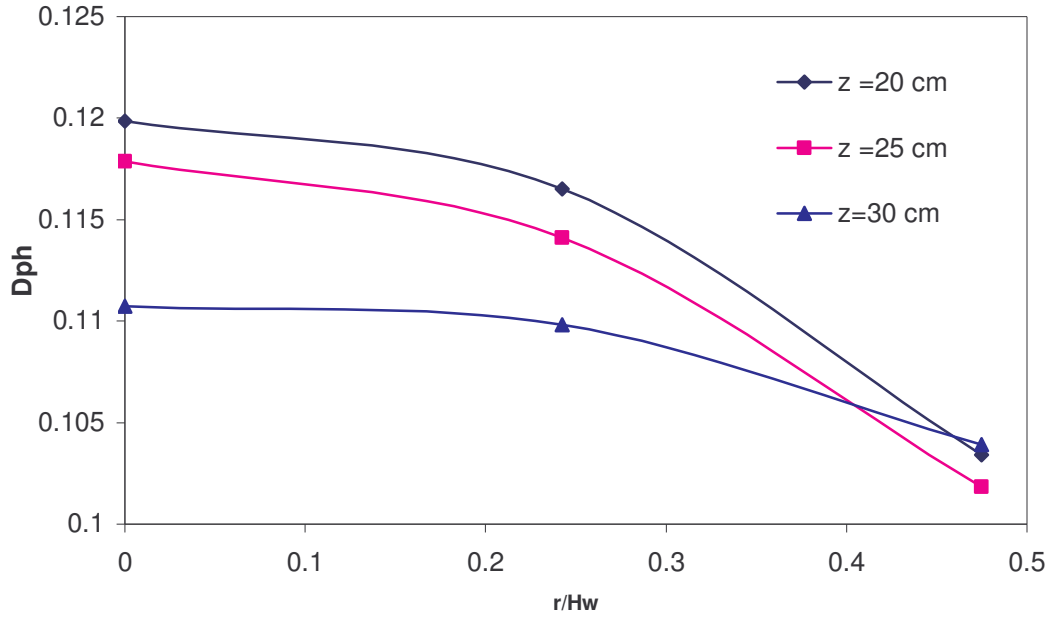

Figure 4.13: Variation of the dispersed slag phase with the dimensionless radial distance at the gas flowrate:0.019m^3/s

In fact, the dispersed oil phase decreased with the radial distance from the centerline towards the wall side of the tank, at different axial distances.

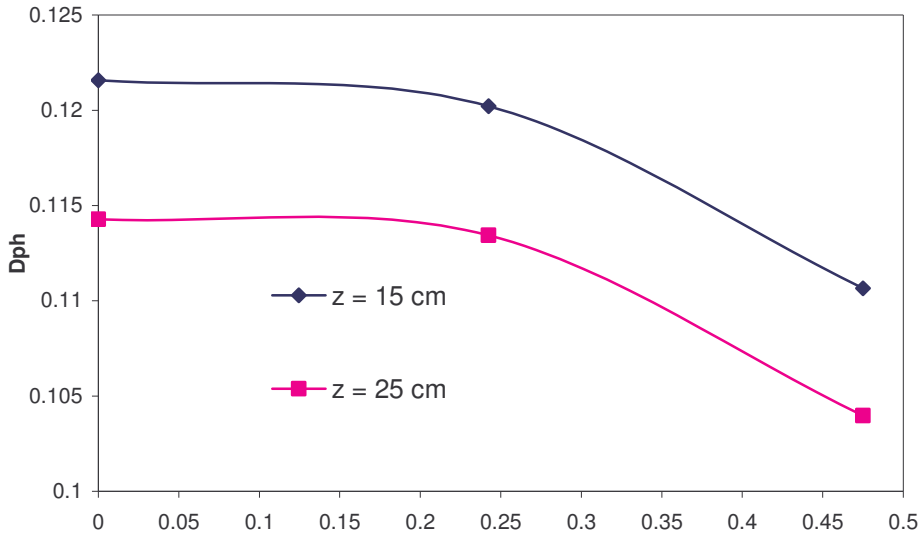

Figure 4.14: Variation of the dispersed phase with the dimensionless radial distance at the gas flowrate:0.014m^3/s.

That effect could be justified by the decrease in turbulence and bubbles dispersion from the plume zone towards the recirculation region. There was a similarity in the dispersion of drops and bubbles within the bath since both were governed by the same principles [40].Five nozzles are located on the right side of the vessel for the compressed air injection into the bath that generated an intensively turbulent water plume zone. In the plume zone (center of the tank till the radial distance $r = 10$ cm), eddies are much larger than of the wall side ($r = 19$ cm).Oil drops were subjected to stronger buoyancy in the plume zone to such extent that their surface tension and gravity were minimal. Much of the kinetic energy of the fluid in the CLU model was associated with the large eddy. In the recirculation zone, viscous forces and drag forces were much more significant. Bubbles were rare in that zone due to the discontinuity of size eddy except when the flow rate was higher [8].

The presence of the top layer (simulated slag) affected the fluid dynamics. It weakened the turbulence motion in the axial and radial directions in the recirculation region but intensified the turbulence motion in the plume region. The axial turbulence fluctuations near the centerline became smaller as the radial distance increased in the recirculation region. The Reynolds shear stress vanished in that region due to the entrainment of oil [53] and that observation agreed well with the result of the current work in the fact that the turbulence intensity decreased from the water plume region towards the wall side.

Marco and Schwerdtfeger [56] argued in their finding which focused on the characteristics of eccentric bubble plumes in liquids, that the flow pattern in radial axis is highly meandering and nonstationnary. It is mainly towards the plume at medium heights and bottom of the vessel. Likewise, Admire investigations [22] confirmed that mass transfer rates in the middle of the bath were greater as a result of an increase in the mean rising plume velocity. On the other hand, Lee and Sohn [37] pointed out that the decrease in the radial dispersed phase was due to the conical shape of the plume. In the CLU model, the water plume was shaped in great part on the right side and bent on the left side such that, bubbles frequency was less pronounced in that zone .

However, the radial dispersed phase did not vary significantly on the left side of the tank because of the weakened turbulence and the formation of dead zones. Ilegusi et al [58] stated that the drag force slows down the bubbles and attenues the intensity of the recirculation flow that ensues. The turbulence on the left side was lesser such that the flow at the free surface was weakened, and such phenomena varied with the flow gas flow rate. The streamlines made by liquid phases were akin to a waterfall.

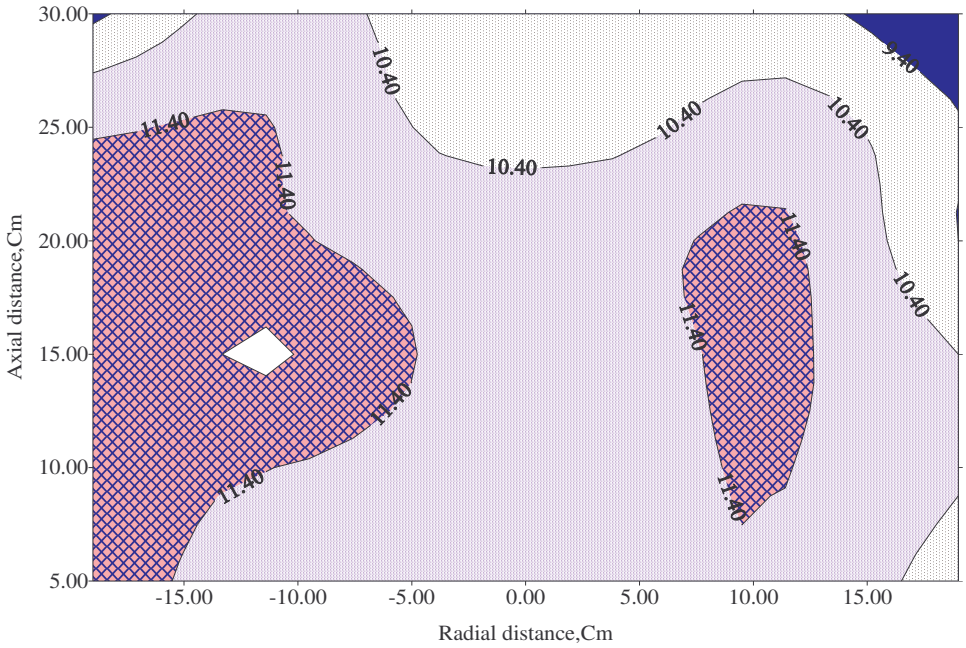

Figure4.15: Dispersed slag phase holdup at the gas flowrate:0.0145m^3/s

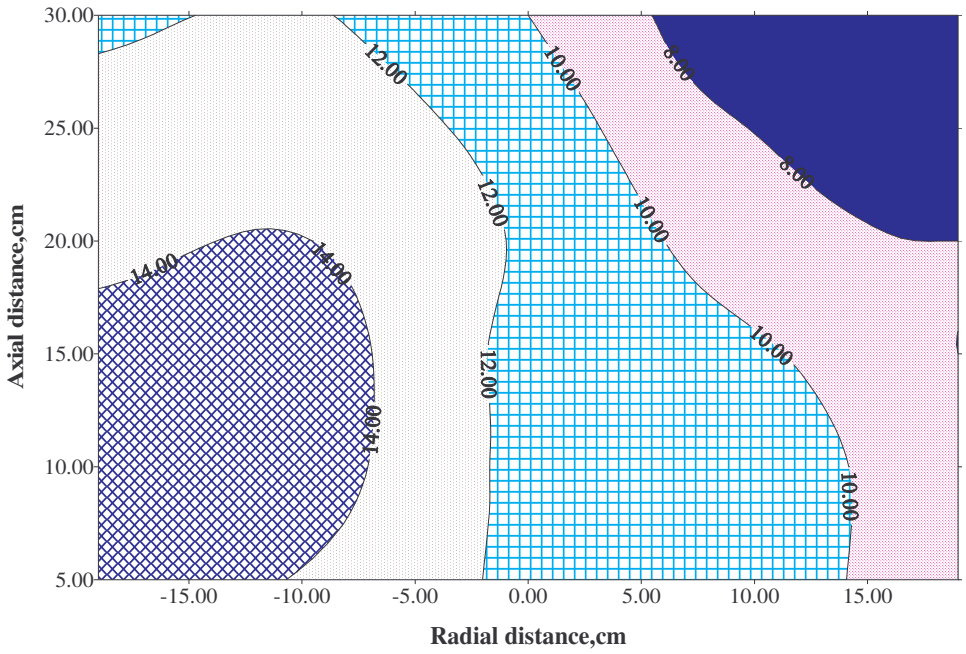

Figure 4.16: Dispersed slag phase holdup at the gas flowrate:0.01m^3/s.

For simplicity reason, the dispersed phase is expressed in percentage in Figures 4.15 and 4.16.

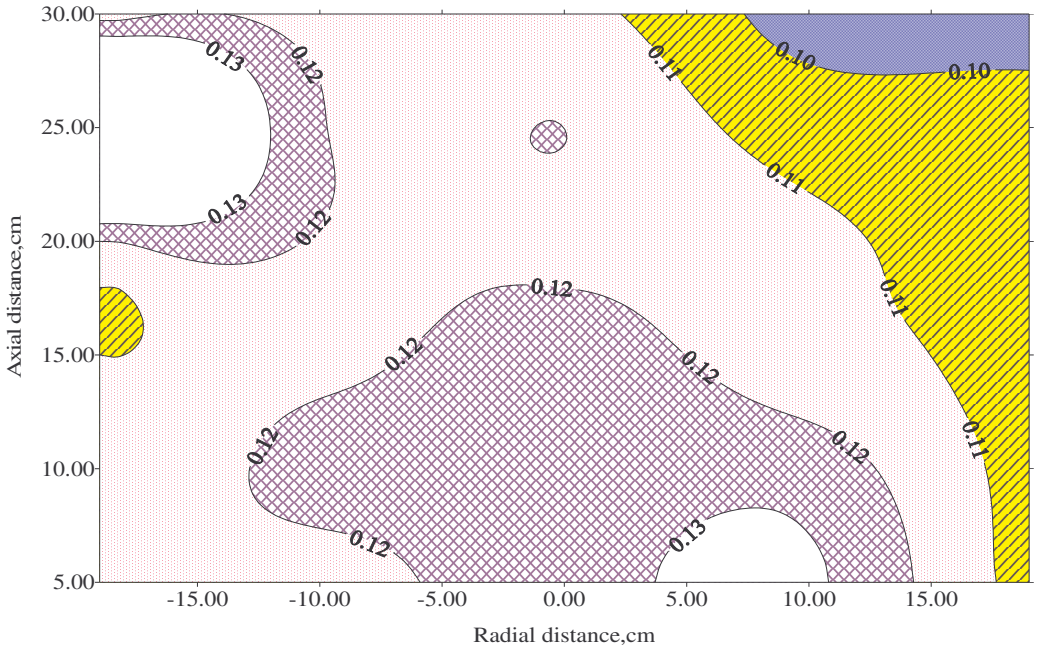

Figure 4.17: Dispersed slag phase holdup at the gas flow rate 0.019m^3/s

The contours displayed in Figures 4.15, 4.16 and 4.17 correlated the dispersed phase to the axial and radial positions. As could be observed, the top surface of the bath and the plume region exhibited greater dispersion than the wall side. The software Surf.6 was used in plotting the contours. More comments are summarized in appendix G.

4.5 Variation of the dispersed phase with the height of the bath

The bath height plays a key role in the mixing intensity and homogenization of the bath. The effect of the height of the bath on the dispersed phase was studied by varying the height of the bath (water and paraffin) between 0.435 m and 0.659 m while the gas flow was kept constant. Figure 4.18 depicts the dispersed phase as a function of the bath height. As can be observed from Figure 4.18, increasing bath height reduced slag dispersion in the tank. This may be explained by obvious reasons such as the decrease of the agitation and turbulence due to the reduced plume radius at the surface. The trend at the radial distance of 9.7 cm under the angle of 90 degrees

displays a sudden increase in the hold-up at the bath height of 54.6 cm as a result of intense turbulence in the water plume region.

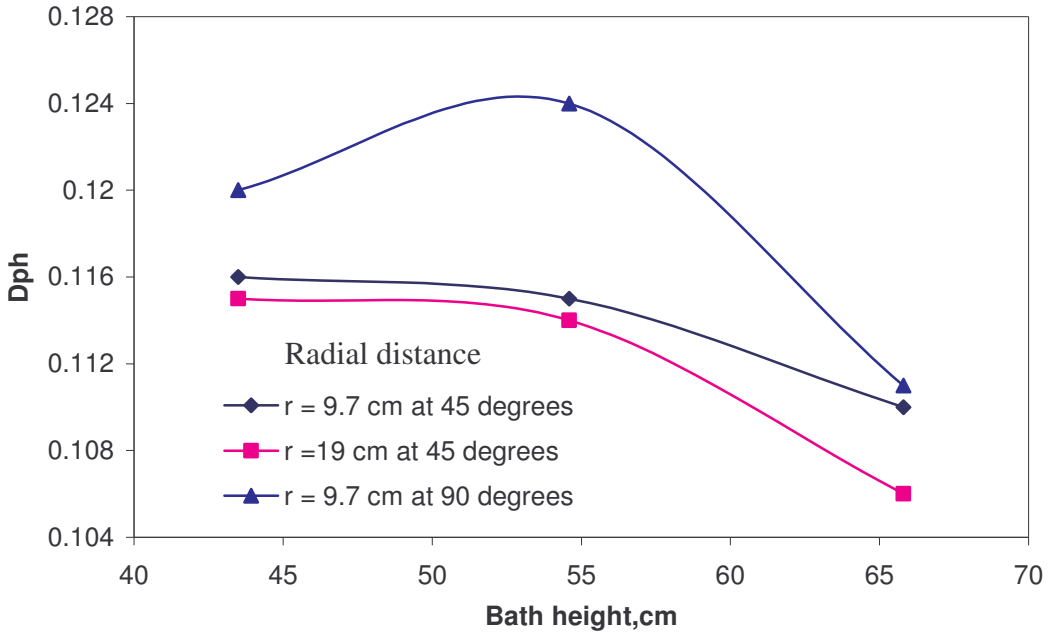

Figure 4.18: variation of the dispersed phase with the relative height of the bath. ($z = 25$ cm;0.019m^3/s)

In fact, at the same gas flow rate, the plume cone was much more enlarged at lower bath height.Accordingly, greater circulation flows were visual at lower bath rather than elevated one. This result showed agreement with earlier work. Observations made by Akdogan and Eric [39], revealed that decreasing bath height intensified the dispersion of oil drops in bath .On the other hand, observations made by K.Iyer and H.Y.Sohn [51] ascertained that increasing the bath height of the light phase leads to an increase in the damping effect on the gas plume and to increasing cross sectional area of the fluid flow, leading to the reduction in the recirculatory flow. In addition to that, K.Murthy and Mehrothra [55] found that the plume cone increased with increasing gas flow rate and decreased with increasing bath height. As a result, agitation and turbulence diminished as the bath height increased, dead volumes increased as well. The higher interfacial tension made the dispersion of oil difficult at elevated bath.

Admire [22] argued that increasing bath height implied a decrease in the bubble formation. In their investigations, Asai et al [59] justified the increased recircuatory loop length in the vessel by an increasing bath height.

4.6 Dimensionless analysis

The operating variables in the current work were defined by the axial distance (z), radial distance (r), gas velocity (v), heights of oil (H_o) and water (H_w). That gave nine variables once they were combined with the physical properties of the liquids. From experimental view point, only the operating conditions were varied such as the gas velocity, the height of water and paraffin, the axial and the radial distances .The physical properties of the liquids were kept fixed. The dispersed slag phase is a function of the following variables z, r, v, H_w, Ho, $\Delta\rho_l$, ρ_g, g, μ.We have three dimensions; length (L), mass (M), time (T). Therefore, by application of Buckingham theorem [52] we get $9-3=6$ dimensionless groups as shown through the dimensional set. Table 8 displayed the dimensional set of the dispersed phase

Table 8: Dimensional set of the dispersed phase

	r	z	H_o	H_w	v	$\Delta\rho_l$	ρ_g	g	μ
L	0	0	0	0	0	1	1	0	1
M	1	1	1	1	1	-3	-3	1	-1
T	0	0	0	0	-1	0	0	-2	-1
π_1	1	0	0	0	0	0	0.667	0.333	-0.667
π_2	0	1	0	0	0	0	0.667	0.333	-0.667
π_3	0	0	1	0	0	0	0.667	0.333	-0.667
π_4	0	0	0	1	0	0	0.667	0.333	-0.667
π_5	0	0	0	0	1	0	0.334	-0.334	-0.334
π_6	0	0	0	0	0	1	-1.001	0.001	0.001

Where, $\Delta\rho_l$, g, μ represent the density difference of liquid phases, acceleration due to gravity and dynamic viscosity.

The dimensional set of the dispersed phase is composed of the following matrices,

- A= [1 0 1;-3 1 -1; 0 -2 -1]
- Matrix unit
- Inverse matrix A^{-1}
- Matrix B

A^{-1} = -1.0000 -0.6667 -0.3333
-1.0000 -0.3333 -0.6667
2.0000 0.6667 0.3333

B= [0 0 0 0 0 1; 1 1 1 1 1 -3; 0 0 0 0 -1 0]

The dimensionless group π is found by figurating out the matrix C.

$$C = -\left[B^T.\left(A^{-1}\right)^T\right] \quad [23]$$

The letter T in the equation above indicates the transposed matrix.

There are six dimensionless groups that are relevant to the process, which can be written as follows;

$$\pi_1 = r.\rho_g^{0.6667}.g^{0.3333}.\mu^{-0.6667} \quad [24]$$

$$\pi_2 = z.\rho_g.^{0.6667} g^{0.3333}.\mu^{-0.6667} \quad [25]$$

$$\pi_3 = H_o.\rho_g^{0.6667}.g^{0.3333}.\mu^{-0.6667} \quad [26]$$

$$\pi_4 = H_w.\rho_g^{\,0.6667}.g^{\,0.3333}.\mu^{-0.6667} \quad [27]$$

$$\pi_5 = v.\rho_g^{\,0.3334}.g^{\,-0.3334}.\mu^{-0.3334} \quad [28]$$

$$\pi_6 = \Delta\rho_l.\rho_g^{\,-1.001}.g^{\,0.0001}.\mu^{0.0001} \quad [29]$$

Dividing all the dimensionless groups by π_4 yields

$$\frac{\pi_1}{\pi_4} = \frac{r}{H_w} \quad [30]$$

$$\frac{\pi_2}{\pi_4} = \frac{z}{H_w} \quad [31]$$

$$\frac{\pi_3}{\pi_4} = \frac{H_o}{H_w} \quad [32]$$

$$\frac{\pi_5}{\pi_4} = \frac{v}{H_w}\rho_g^{\,-0.3333}.g^{\,-0.6667}.\mu^{0.3333} \quad [33]$$

$$\frac{\pi_6}{\pi_4} = \frac{\Delta\rho_l}{H_w}.\rho_g^{\,-1.6667}.g^{\,-0.3333}.\mu^{0.6667} \quad [34]$$

By squaring the dimensional group [33] and combining with [34], we get the dimensional group called Modified Froude Number [35]

$$\frac{\pi_5{}^2}{\pi_6.\pi_4} = \frac{\rho_g}{\Delta\rho_l}\left(\frac{v^2}{g.H_w}\right) \qquad [35]$$

Hence, the overall correlation of the dispersed phase can be defined at last as a mathematical function of four dimensionless groups as follows:

$$Dph = f\left[\frac{z}{H_w}, \frac{r}{H_w}, \frac{H_o}{H_w}, N_{Fr}\right] \qquad [36]$$

The form of the overall correlation of the dispersed slag phase may be determined through further fitting approaches, by either polynomial or non linear regression.

4.7 Dispersed slag phase model

Assuming that the dispersed slag phase is defined at the centerline of the bath by ϕ_{cent}, the corresponding rate of emulsion at any position within the bath from the center can be estimated through a model of the dispersed slag phase.

The current model may be defined as a mathematical expression that regroups the value of the holdup at the centerline and all relevant dimensionless groups such as the axial distance from the original interface, the relative height of the liquids, the radial distance and the modified Froude number. In this case, the axial and radial distances are given as ratios to H_w. Mathematically, the following expression may be written when the volume of the gas is ignored,

$$\phi = f\left(\frac{z}{H_w}, \frac{r}{H_w}, \frac{H_o}{H_w}, N_{Fr}\right) \qquad [37]$$

M.S.Lee and H.Sohn [37] investigation correlated the dispersed phase in the water plume zone as a Gaussian distribution. Akdogan and Eric [38] have found an equation that fit to a number of the present experimental data, precisely in the water plume zone. The main difference lies on discrepancy of the results in the vicinity of the wall side and their coefficient of multiple regressions was 0.87 when using the previous model. The following equation was used as an expression of the dispersed phase,

$$\phi(z.r) = \phi_{Centerline}\left[1-\left(\frac{r}{H_w}\right)^2\right]^a + \sin\left[b\left(\frac{r}{H_w}\right)\right] \qquad [38]$$

According to the previous investigation [38], the model should fit well when the rate of slag emulsification increased with the radial distance. On the contrary, the opposite effect was observed on the right side in the current work. The model of the dispersed phase was defined as shown in appendix F according to the experimental data.

For reasons mentioned above, the model suggested by Akdogan and Eric was subject to a revision and improvement in order to establish a relationship that best fit experimental data of the current work. First of all, the following expression from earlier work is suppressed,

$$\left[Sin\frac{br}{H_w}\right] \qquad [39]$$

The reason is that this trigonometric function increases with the radial distance. Secondly, the estimate initial value of the exponent a is taken as 0.4.

As can be seen from Tables 9A and 9 B, the coefficient (a) depends on the sampling position, on the modified Froude Number and the bath height.
Mathematically, the coefficient a may be expressed as follows;

$$a = \left(\frac{z}{H_w}\right)^m (N_{Fr})^n \left(\frac{H_o}{H_w}\right)^p \quad [40]$$

Powers m, n and p are determined by multiple regressions based on experimental data.

The software Mat lab was used at this step in solving the set of equations.

Hence,

$m = -0.3851$

$n = 0.2610$

$p = 1.0661$

Therefore, $a = \left(\frac{z}{H_w}\right)^{-0.3851} (N_{Fr})^{0.2610} \left(\frac{H_o}{H_w}\right)^{1.0661}$

The model of the dispersed slag phase was defined as shown in appendix F by the following equation,

$$Y = a * F_2 \quad \ldots\ldots [41]$$

Where,

$$F_2 = F_1^b \quad \ldots\ldots [42]$$

$$F_1 = 1 - x^2 \quad \ldots\ldots [43]$$

The variable x represents the dimensionless radial distance $\left(\frac{r}{H_w}\right)$

By performing non linear regression, important statistical results were selected as listed in appendix F. The standard error of the estimate and the coefficient of multiple regression were 3.7×10^{-4} and 0.97 whilst the standard deviation averaged was

0.0004.That showed good agreement between the calculated and the experimental data with a proportion of variance of 98 %

The equation of the dispersion model may be approximated by the following mathematical expression;

$$\phi_{(z.r)} = \phi_{cent}\left[1-\left(\frac{r}{H_w}\right)^2\right]^a \qquad [44]$$

$$\phi_{centerline} = 0.22\left[(Nfr)^{0.12}\left(\frac{H_o}{H_w}\right)^{0.74}\left[1-\left(\frac{z}{H_w}\right)^2\right]^{0.483}\right]^{1.02} \qquad [45]$$

The above model was defined by means of the software data fit version 8.1.69. The coefficient of multiple regression R^2=0.97 and standard error of the estimate was 3.7×10^{-4} .The solver was nonlinear regarding various trends found during experimental evaluation. Previous expression of the centerline dispersed phase was adopted since the relevant dimensionless groups at the centerline namely axial distance, height ratio of liquid phases and the modified Froude number were similar in both investigations. Figures 4.19, 4.20, 4.21 and 4.22 highlight how close the experimental results are from the calculated ones from the center towards the wall side.

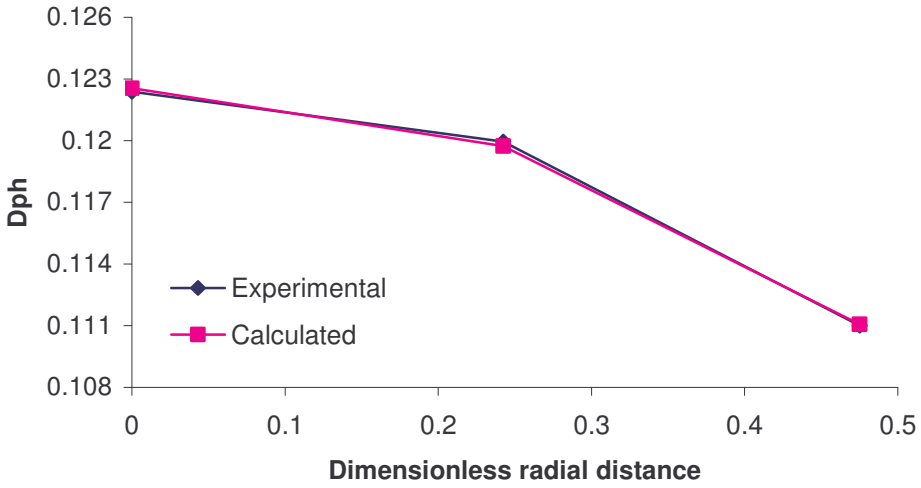

Figure 4.19: The correlation of radial dispersed phase: experimental and calculated values ($z = 20\,\text{cm}$)

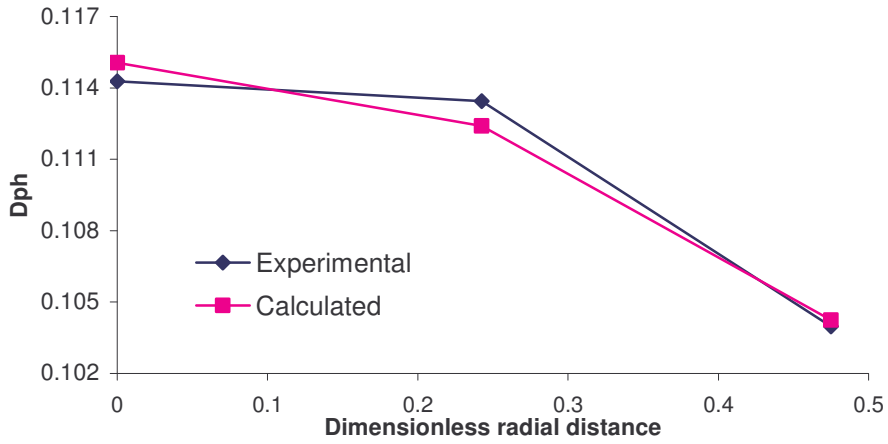

Figure 4.20: The correlation of radial dispersed phase: experimental and calculated values (z= 25 cm)

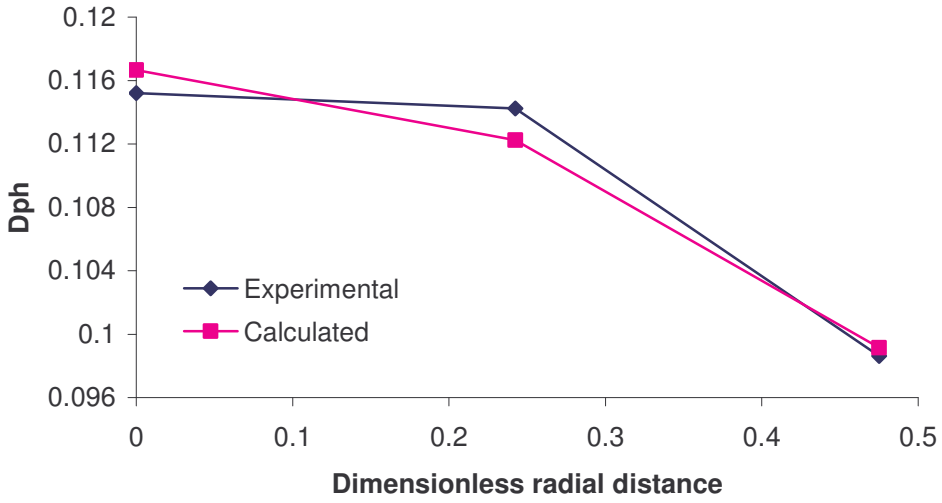

Figure 4.21: The correlation between experimental and calculated radial dispersed phase ($z = 5\,\text{cm}$)

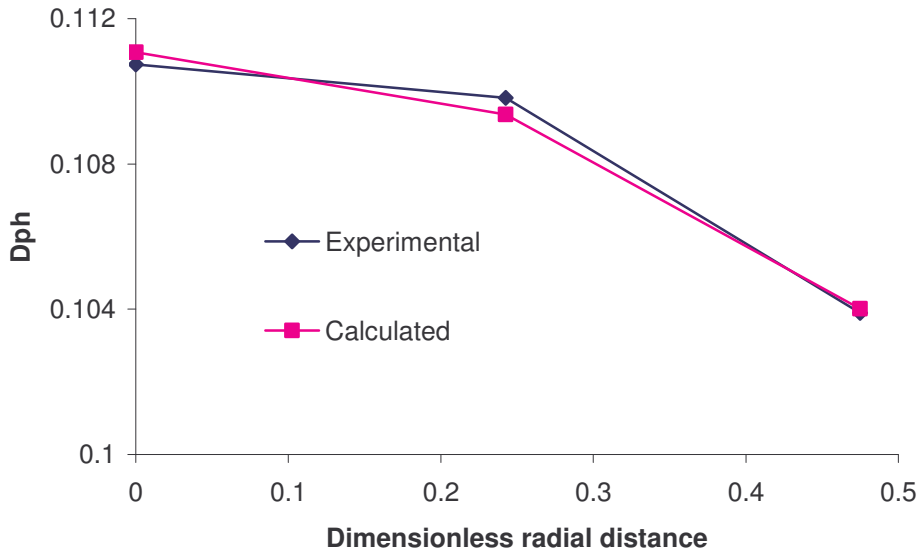

Figure 4.22: The correlation between experimental and calculated radial dispersed phase ($z = 15\,\text{cm}$)

For the model to best fit, the R-squared might tend towards the unity value standard error should be as weak as possible in decimal range. Previous work [1] found the correlation with a coefficient of multiple regression equal to 0.94.That coefficient dropped to 0.87 when fitting the current data to their relationship. Figure 4.23 illustrates a comparison between current work and Akdogan and Eric [38] work in terms of relationship between experimental and correlated model values of dispersed phase hold-up. It is clear that the revised equation used in the present work gives much better correlation between experimental and model values.

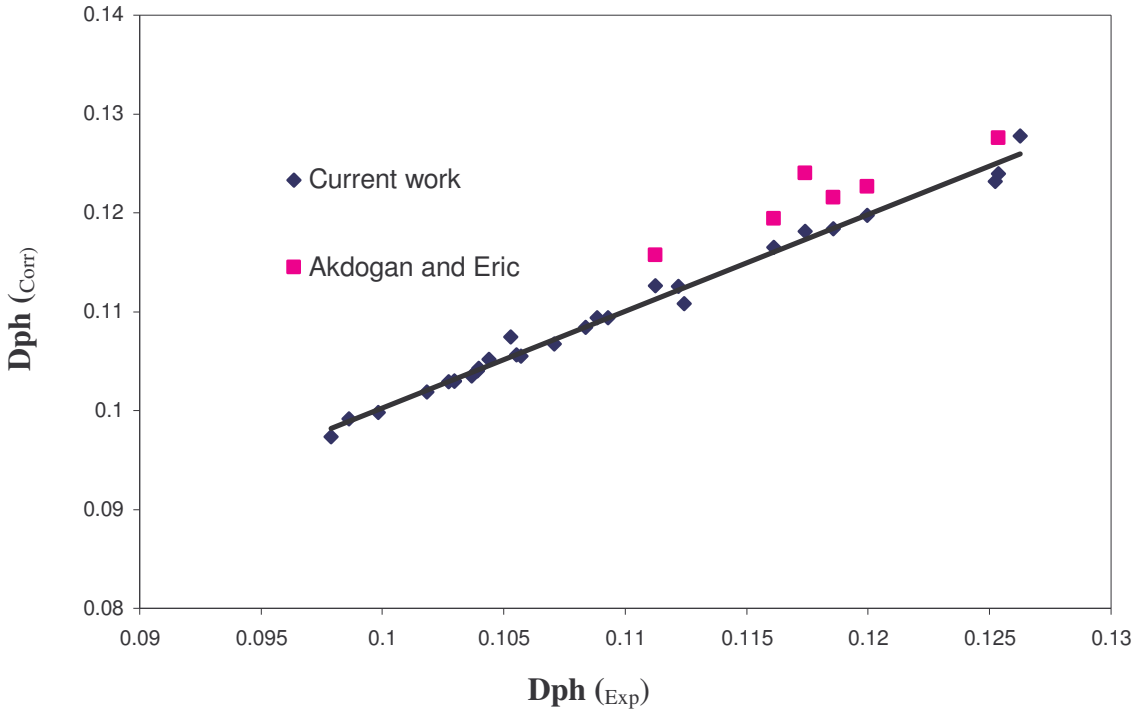

Figure 4.23: Correlation between the experimental and the calculated results

Table 9 A: Fitting results of dispersed slag phase holdup

Bath height (cm)	Gas flow rate (m^3/s)	$\frac{r}{H_w}$	z (cm)	$\phi_{\exp}$	ϕ_{cal}	R^2	a
54.6	0.019	0	10	0.11218	0.11207		
54.6	0.019	0.2425	10	0.10887	0.10902		
54.6	0.019	0.475	10	0.09982	0.09978	0.9995	
54.6	0.019	0	10	0.11218	0.11256		
54.6	0.019	0.2425	10	0.10929	0.10941		
54.6	0.019	0.475	10	0.1123	0.11180	0.93	
54.6	0.019	0	5	0.11243	0.11081		
54.6	0.019	0.2425	5	0.10528	0.10746		
54.6	0.019	0.1745	5	0.09789	0.09732	0.93	
54.6	0.019	0	20	0.12734	0.12835		
54.6	0.019	0.2425	20	0.12535	0.12398		
54.6	0.019	0.475	20	0.11056	0.11092	0.98	
54.6	0.019	0	25	0.12626	0.12778		
54.6	0.019	0.2425	25	0.12522	0.12316		
54.6	0.019	0.475	25	0.10883	0.10938	0.96	
54.6	0.014	0	5	0.1155	0.11448		
54.6	0.014	0.2425	5	0.11123	0.11259		
54.6	0.014	0.475	5	0.10707	0.106373	0.92	0.27
54.6	0.01	0	30	0.12153	0.12166		
54.6	0.01	0.2425	30	0.11856	0.11838		
54.6	0.01	0.475	30	0.10837	0.10842	0.99	0.45
54.6	0.01	0	25	0.12365	0.12311		
54.6	0.01	0.2425	25	0.1174	0.11814		
54.6	0.01	0.475	25	0.10367	0.10347	0.996	
54.6	0.01	0	25	0.12365	0.12576		
54.6	0.01	0.2425	25	0.12344	0.12055		
54.6	0.01	0.475	25	0.1044	0.10519	0.94	0.7
54.6	0.01	0	20	0.11903	0.11874		
54.6	0.01	0.2425	20	0.11611	0.11649		
54.6	0.01	0.475	20	0.10964	0.10954	0.99	0.32

Table 9 B: Fitting results of the dispersed slag phase holdup

Bath height (cm)	Gas flow rate (m^3/s)	$\frac{r}{H_w}$	z (cm)	$\phi_{\exp}$	ϕ_{cal}	R^2	a
65.8	0.019	0	5	0.10636	0.10653		
65.8	0.019	0.2425	5	0.1057	0.10548		
65.8	0.019	0.475	5	0.10212	0.10217	0.992	0.16
65.8	0.019	0	10	0.10654	0.10646		
65.8	0.019	0.2425	10	0.10552	0.10562		
65.8	0.019	0.1745	10	0.10297	0.10295	0.997	0.13
43.5	0.019	0	25	0.11985	0.12020		
43.5	0.019	0.2425	25	0.11651	0.11603		
43.5	0.019	0.475	25	0.10342	0.10355	0.998	0.58
43.5	0.019	0	20	0.11786	0.11798		
43.5	0.019	0.2425	20	0.1141	0.11394		
43.5	0.019	0.475	20	0.10183	0.10187	0.99	0.57
43.5	0.019	0	15	0.11074	0.111082		
43.5	0.019	0.2425	15	0.10982	0.10936		
43.5	0.019	0.475	15	0.1039	0.10401		0.26
43.5	0.01	0	5	0.1152	0.11666		
43.5	0.01	0.2425	5	0.11423	0.11225		
43.5	0.01	0.475	5	0.09862	0.09915	0.96	
43.5	0.014	0	25	0.11428	0.11506		
43.5	0.014	0.2425	25	0.11344	0.11240		
43.5	0.014	0.475	25	0.10397	0.10424	0.97	0.39
43.5	0.014	0	20	0.12238	0.12255		
43.5	0.014	0.2425	20	0.11996	0.11973		
43.5	0.014	0.475	20	0.111	0.11106	0.998	0.38
43.5	0.014	0	15	0.12158	0.12218		
43.5	0.014	0.2425	15	0.12021	0.11940		
43.5	0.014	0.475	15	0.11066	0.11087	0.985	0.38
43.5	0.014	0	10	0.12184	0.12145		
43.5	0.014	0.2425	10	0.11881	0.11933		
43.5	0.014	0.475	10	0.11289	0.11276	0.989	0.3

4.8 Scale up of the dispersed slag phase results to the real CLU reactor

Previous investigators [45, 22, and 72] used the following relation to correlate the mixing time in a reduced scale model to the full scale CLU converter,

$$\lambda^{\frac{1}{2}} = \frac{T_{mix,\mathrm{mod}}}{T_{mix,fs}} \qquad [46]$$

Where λ is the scale factor.

Since tests on the current work were carried in the same vessel, the similar relationship might be applied to extrapolate the dispersed slag phase results to the industrial scale as follows,

$$\lambda^{\frac{1}{2}} = \frac{\phi_{(z,r)\mathrm{mod}\,el}}{\phi_{(z,r)fs}} \qquad [47]$$

The above equation remains valid since the modified Froude correlated the gas injection between CLU-model and CLU prototype.

5. CONCLUSIONS

From a cold model of the CLU reactor, the dispersion behavior of slag phase was investigated at various operating conditions. The following conclusions were drawn;
The dispersed slag phase increased with the gas flow rate. The dispersed phase decreased with the vertical distance from the original interface between liquid phases. The dispersed phase decreased with the radial distance .The dispersed slag phase was inversely proportional to the relative height of liquid phase. The dispersed phase was apparently much more observable on the right side than on the left side. Four dimensionless numbers defined the current model through in mathematical analysis. Amongst parameters; the modified Froude Number ensured the correlation between both model and prototype. The overall correlation of the dispersed simulated slag phase was defined by the following equation

$$\phi_{(z.r)} = \phi_{cent}\left[1-\left(\frac{r}{H_w}\right)^2\right]^a$$

$$\phi_{centerline} = 0.22\left[(Nfr)^{0.12}\left(\frac{H_o}{H_w}\right)^{0.74}\left[1-\left(\frac{z}{H_w}\right)^2\right]^{0.483}\right]^{1.02}$$

The experimental results agreed well with the correlated ones since the standard error of the estimate and R-squared were respectively 3.7×10^{-4} and 0.97 with a proportion of variance of 98 % and standard deviation of 0.0004.

FUTURE WORK

1. For the sake of improving agitation as well as turbulence effects on the left side where dead zones were observed in the upper zone of the bath, it will be worthwhile

to use the top lance. Then, further investigation on the combined blowing effect on the dispersed phase may be undertaken.

2. Gas holdup and bubbles frequency in the CLU vessel have not been investigated yet. To better correlate the fluid dynamics to the emulsification phenomena, a study on such effects is recommended.

3. The dispersed slag phase decreased with the axial distance .Photographic method should be applied in an attempt of gathering images of the emulsion at various axial distances in the water plume zone and in the recirculation zone.

6. REFERENCES

1. P.Kozakevitch, Foams and Emulsions in Steelmaking, *Journal of Metals*, July1969, 57-67.
2. M.J.Rosen, *Surfactants and interfacial phenomena*, New York, 1978.
3. H.Schubert, Surface Phenomena Effects in Liquid /Liquid Mixing; *AICHE-Meeting.Los Angeles*, 12 –17 Nov. 2000.
4. T.Lemenand, D.Della Valle and Y.Zellouf, International Journal of Multiphase flow 29(2003), 814-18, Elsevier Science, France.
5. Z.Lin and R.I.L.Guthrie, *Metallurgical Transactions B*, 1994, Vol.25B, 855-864.
6. H.Shahrokhi and J.M.Shaw, *Chemical Engineering Science*, Vol.49, no24B pp.5203-5213.
7. Tanaka and Guthrie, *6th Process Technology Conference Proceedings*, April, 1986, pp.249 – 255, Washington, D.C, U.S.A
8. M.Martin and M.Diaz: *Chemical Engineering Communications*, 2002, Vol.189 (4), pp543-70.
9. C.Moore and R.Marshall, *Steel making*, The Institute of Metals, 1991.
10. E.T.Turkdogan, *Minerals Sci. Engineering*, Johannesburg, South Africa Vol.8, No2, (April) 1976, 94-95.
11. D.Poggy, R.Minto and W.G.Davenport, Mechanism of Metal Entrapment in Slag, *Journals of Metals*, November 1969, 40- 45.
12. Thomas Szirtes: *Applied Dimensional Analysis and Modeling*, 1997, pp.790.
13. E.Fritz and W.Gebert, *Canadian Metallurgical* Quarterly, Vol.44, No2, pp.249 260, 2005.
14. Z.Han and Holappa: *ISIJ International,* Vol.43 (2003), No.3, pp.292-297.
15. M.G.Frohberg and G.Hanschuh, Studies on the modeling of the emulsion in the Bottom blowing converter, *Neue Hutte*, December (Vol.33), No12, pp.447- 451, 1998.
16. Martin, M.Rendueles and M.Diaz, *Canadian Journal of Chemical Engineering,* Vol.82, April 2004, pp.249-255.
17. S.C.Koria and M.R.R.I.Shamsi, *Iron making and Steel making 1990*. Vo.17.

No6, 402.

18. E.Gopal, *Emulsion Science*, AP (1968), London and New York.
19. D.K.Panda and D.Robertson, *Steelmaking Conference Proceedings*, 1994, pp.443-456.
20. D.J.Price, Institute *of Mining and Metallurgy*, London (1974), pp.8-15.
21. H.W.Meyer, W.F.Porter, G.C.Smith and J.Szekely, Slag-Metal Emulsions and Their importance in BOF Steelmaking, *Journal of Metals*, July1968, 35-42.
22. A.Chaendera, MSc Dissertation (2006), Effects of the simulated slag phase on Mixing and Mass Transfer Rates in a Creusot Loire Uddeholm Converter Model, University of the Witwatersrand, South Africa.
23. D.Phelan and G.Brooks, *Proceedings of Materials 98*, the biennial Conference of the Institute of Materials Engineering, Australasia.
24. Fabritius.T, P.Mure and J.Harkki, *Modeling of bath oscillation in the A.OD*, Laboratory of Process Metallurgy. Department of Process and Environment Engineering, University of Oulu, Finland, pp.1-16.
25. O.Johnson and Oberg, *Secondary steelmaking*, London.1977, Proceedings, 88
26. S.Yamashita and M.Iguchi, *ISIJ International*, Vol.43 (2003), pp.1326-1332
27. M.Martin, M.Rendueles and M.Diaz, Steel – Slag mass transfer in steel converter, Bottom and top/bottom combined blowing through cold model experiments, *Chemical Engineering Research and Design*, 2005, 83(A9), 1076-1084.
28. R.P.Singh and D.N.Ghosh, *Ironmaking and steelmaking*, Vol.17 (5), pp.333, 1990.
29. A.Zaidi and H.Sohn, Measurement and correlation of drop size distribution in Liquid –liquid emulsions formed by high velocity bottom gas injection, *ISIJ International*, Vol.35 (1995), No3, pp.234-241.
30. E.T.Turkdogan: *Advances in extractive Metallurgy*, Eds. Plenum, New York, 1979.
31. T.Wei and F.Oeters, A model test for emulsion in gas stirred ladles, *Steel research 63*, 1992, No2, pp.60-68.
32. W.Kleppe and F.Oeters, *Arch.Eisenhuttenwes.47,* M*ay* No5, pp.271-275, 1976
33. K.Shinoda, Emulsions and Solubilization, New York, 1986.

34. Subagyo, A. Brooks, K.S.Coley and G.A.IRONS, Generation of Droplets in Slag – Metal Emulsions through Top Gas Blowing, ISIJ International, Vol.43 (2003), No7, pp.983-989.

35. G.Brooks, Y.Pan, Subagyo and K.Colley, Modelling of trajectory and residence Time of metal droplets in slag-metal –gas emulsions in oxygen steelmaking, *Metallurgical and Materials Transactions B,* Vol.36B (2005), pp.525-535.

36. G.Reiter and K.Schwerdtfeger, *I.SI.JInternational*, vol32 (1992), No1, 50-56.

37. M.S.Lee and H.Y.Sohn, *Metallurgical and Materials transactions B, Vol.27 B*, 1996, pp.213- 219.

38. G.Akdogan and R.H.Eric, Physical Modeling of Slag-metal Dispersion, *VII International conference on molten slag fluxes and Salts*, 2004, pp.671- 7.

39. G.Akdogan and R.Eric, *Metallurgical Transactions B*, Vol.30B, 19, pp.231-239

40. J.Szekely: *Fluid Flow Phenomena in metals Processing*, New York: Academic, 1979.

41. W.J.Duncan, *Physical similarity and dimensional analysis*, London, 1953.

42. S.Koria and K.Lange, *Metallurgical and Materials Trans.B*, Vol15B, March 1984,109.

43. S.C.Koria and A. George, *Iron making and steel making 1988*, Vol.15. No3, 127.

44. S.KIM and R.S.Fruehan, *Metallurgical and Materials Trans.B*, Vol.18B, June 1987,382.

45. Nyoka, Mixing and Mass Transfer in a Creusot Loire Uddeholm converter, *Thesis* (2001), *University of the Witwatersrand*, South Africa.

46. W.E.Baker, P.Westine and F.Dodge, *Similarity methods in engineering Dynamics*, 338-42.

47. A.C.Fowler, Mathematical *Models in the Applied Sciences*, Cambridge University, Press1997, 3.

48. B.David, Mathematical Modelling, London: Prentice Hall, 1996.

49. M.Zlokarnik, *Chemical Engineering Science*, Vol.53, No17, 3030.

50. S.Ghorai, G.G.Roy and S.K.Roy, Submerged liquid Slag injection in Steel melt, *Ironmaking and Steelmaking* (2004), Vol.31, pp.401-408.

51. K.M.Iyer and H.Y.Sohn, *Metallurgical and Materials Transactions 25B,* 1994,

pp.207-19.

52. R.I.L.Gutrie, *Engineering in Process Metallurgy*, 1992.
53. M.Iguchi, O.Ilegusi, H.Ueda, T.Kuranaga and Z.Morita, *Metall.Trans.B* (1996), Vol.27B, pp.35-41.
54. S.J.Buckler, D.E.Langberg and D.R.Swinbourne, Measurement of Total Gas-Liquid Interfacial Area during Submerged Gas Injection into a Liquid Bath, *EPD Congress* 2002, pp.477- 490.
55. K.Murthy and Mehrothra, *Ironmaking and Steelmaking*, Vol.19 No5 (1992), pp.377-389.
56. M.Castello-Branco and K.Schwerdtfeger, *Metallurgical and Materials Transactions B*, Vol.27B, 1996, pp.231-39.
57. P.Anagbo and J.Brimacombe: *Metallurgical and Materials Transactions B* (1990), Vol.21B, 637-648.
58. Ilegusi, M.Iguchi, K.Nakajima, M.Sano and M.Sakamoto, *Metallurgical Transactions B*, Vol.29 B, 1998, pp.211-222.
59. S.Asai, M.Kawachi and I.Muchi: Scaninject III, Lulea, Sweden, no12, 1983, pp.1-29.
60. O.Johnsson and K.Oberg, Secondary Steelmaking, 1978, Metals Society, London.
61. R.Clift, G.John and W.Martine, *Bubbles, Drops and Particles*, Academic Press 1978, USA.
62. P.Anagbo and J.Brimacombe, *Metallurgical and Materials Transactions B*, Vol.21 B (1990), pp.637-648.
63. V.Sahajwalla et al*: Metallurgical Transactions B,* Vol.21B, 1990, pp.71-80.
64. R.I.L.Guthrie, M.Isac and Z.Lin, *Ironmaking and Steelmaking*, April (2005), Vol.32, No2, pp.133-140.
65. L.Theo, P.Koros, V.Ramachandran, *International Symposium on Injection in Process Metallurgy (*1991), Vol.2, New Orleans, Warrendale, TMS.
66. C.Smith, *Formulation and optimization of mathematical models*, Scranton, Pa.International textbook, 1970,430.
67. R.H.Tupkary, *Introduction to modern steelmaking*, Khanna Publ.Delhi, 317.
68. Y.Chung and A.W.Cramb, *Metallurgical and Materials Trans.B*, vol31B, 957-

71.

69. B.V.Patil, A. Chan and R.J.Choulet, *Steelmaking and refining volume*, 715-18

70. Annie Nordquist and Par Jonsson, Royal Institute of Technology, Sweden.

71. F.Qian, R.Mutharasan and B.Farouk, *Metall.TransB*, vol27B, 1996, 911-20.

72. W.Hoyle*, Pilot plants and scale up of chemical processes* II, 28.

73. B.Deo, A.Karamcheti, A.Paul, P.Singh and R.Chhabra, *Characterization of Slag – Metal Droplet – Gas Emulsion in Oxygen Steelmaking Converters, ISIJ International,* Vol.36 (1996), no6, pp.658-666.

APPENDICES

Appendix A1: Values of the dispersed slag phase at various flow rates along the radial axis situated at 90 degrees (Bath height: 43.5 cm; radial distance =19 cm)

Gas flow rate m^3/s	*r cm*	*Axial distance cm*	*Meas1 Dph*	*Meas2 Dph*	*Meas3 Dph*	*Meas4 Dph*	*Meas5 Dph*	*Meas6 Dph*	*Meas7 Dph*	*Meas8 Dph*	*Av.*
0.01	19	5	0.087	0.080	0.071	0.086	0.073	0.073	0.077	0.090	0.080
0.01	19	10	0.083	0.086	0.083	0.081	0.083	0.103	0.076	0.09	0.086
0.01	19	15	0.09	0.083	0.086	0.098	0.085	0.077	0.082	0.078	0.085
0.01	19	20	0.073	0.070	0.088	0.089	0.080	0.083	0.069	0.082	0.079
0.01	19	25	0.078	0.07	0.048	0.076	0.055	0.05	0.064	0.052	0.062
0.01	19	30	0.069	0.094	0.045	0.058	0.102	0.068	0.068	0.069	0.072
0.014	19	5	0.09	0.099	0.094	0.09	0.095	0.095	0.083		0.093
0.014	19	10	0.096	0.104	0.1	0.105	0.100	0.096	0.089	0.095	0.098
0.014	19	15	0.100	0.071	0.094	0.088	0.100	0.102	0.100	0.101	0.095
0.014	19	20	0.096	0.071	0.073	0.095	0.081	0.103	0.099	0.078	0.087
0.014	19	25	0.095	0.080	0.070	0.083	0.086	0.070	0.081	0.068	0.079
0.014	19	30	0.074	0.061	0.067	0.078	0.068	0.069	0.078	0.057	0.069
0.019	19	5	0.111	0.102	0.113	0.103	0.111	0.100	0.105	0.109	0.107
0.019	19	10	0.111	0.112	0.105	0.113	0.111	0.102	0.098	0.103	0.107
0.019	19	15	0.111	0.106	0.120	0.100	0.113	0.12	0.116	0.119	0.113
0.019	19	20	0.106	0.113	0.097	0.109	0.105	0.112	0.114	0.104	0.108
0.019	19	25	0.100	0.113	0.098	0.111	0.111	0.108	0.093	0.111	0.106
0.019	19	30	0.100	0.096	0.085	0.105	0.103	0.089	0.101	0.100	0.098

STDEV	*0.07*	*0.08*	*0.007*	*0.008*	*0.012*	*0.018*	*0.005*	*0.005*	*0.011*	*0.013*	*0.009*
	0.008	0.005	0.006	0.007	0.006	0.008	0.007				

The standard deviation in row related to the dispersed phase in appendix A1.

Appendix A2: Values of the dispersed slag phase at various flow rates along the radial axis situated at 135 degrees (Bath height: 43.5 cm; radial distance =19 cm)

Gas flow rate m^3/s	*r* *cm*	*Axial distance* *cm*	*Meas1* *Dph*	*Meas2* *Dph*	*Meas3* *Dph*	*Meas4* *Dph*	*Meas5* *Dph*	*Meas6* *Dph*	*Meas7* *Dph*	*Meas8* *Dph*	*Av.*
0.01	19	5	0.089	0.101	0.100	0.104	0.109	0.108	0.095	0.083	0.099
0.01	19	10	0.107	0.096	0.103	0.089	0.082	0.103			0.097
0.01	19	15	0.103	0.088	0.088	0.109	0.103	0.0885	0.085	0.086	0.094
0.01	19	20	0.085	0.086	0.096	0.077	0.088	0.087	0.086	0.105	0.089
0.01	19	25	0.095	0.095	0.085	0.089	0.069	0.103	0.095	0.078	0.088
0.01	19	30	0.069	0.052	0.068	0.103	0.086	0.093	0.086	0.103	0.083
0.014	19	5	0.084	0.093	0.094	0.101	0.087	0.089	0.095	0.092	0.092
0.014	19	10	0.095	0.100	0.108	0.105	0.104	0.109	0.106	0.103	0.104
0.014	19	15	0.103	0.104	0.104	0.101	0.106	0.116	0.114	0.105	0.107
0.014	19	20	0.097	0.094	0.087	0.089	0.094	0.103	0.082	0.085	0.091
0.014	19	25	0.078	0.102	0.103	0.088	0.086	0.096	0.095	0.102	0.094
0.014	19	30	0.076	0.086	0.086	0.069	0.068	0.103	0.078	0.085	0.081
0.019	19	5	0.113	0.108	0.115	0.119	0.118	0.110	0.117	0.114	0.114
0.019	19	10	0.122	0.107	0.110	0.110	0.116	0.105	0.111	0.116	0.112
0.019	19	15	0.122	0.093	0.113	0.106	0.100	0.102	0.111	0.114	0.108
0.019	19	20	0.098	0.105	0.100	0.095	0.108	0.097	0.096	0.109	0.101
0.019	19	25	0.094	0.104	0.108	0.096	0.104	0.106	0.104	0.102	0.102
0.019	19	30	0.097	0.107	0.103	0.101	0.093	0.100	0.111	0.105	0.102

APPENDIX A3: Values of the dispersed slag phase at various flow rates along the radial axis situated at 90 degrees (Bath height: 43.5 cm, radial distance 9.7 cm).

Gas flow rate m^3/s	*Radial distance* cm	*Axial distance* cm	*Meas1 Dph*	*Meas2 Dph*	*Meas3 Dph*	*Meas4 Dph*	*Meas5 Dph*	*Meas6 Dph*	*Meas7 Dph*	*Meas8 Dph*	*Av.*
0.01	9.7	5	0.114	0.101	0.106	0.118	0.115	0.113			0.111
0.01	9.7	10	0.118	0.103	0.104	0.112	0.103	0.120	0.122	0.115	0.112
0.01	9.7	15	0.097	0.114	0.109	0.089	0.122	0.094	0.096	0.100	0.103
0.01	9.7	20	0.097	0.091	0.113	0.115	0.073	0.077	0.092	0.083	0.093
0.01	9.7	25	0.102	0.090	0.090	0.070	0.073	0.086	0.070	0.071	0.082
0.01	9.7	30	0.054	0.047	0.053	0.053	0.045	0.098	0.061	0.052	0.093
0.014	9.7	5	0.116	0.105	0.106	0.113	0.118	0.118	0.113	0.103	0.111
0.014	9.7	10	0.12	0.105	0.107	0.113	0.112	0.114	0.103	0.103	0.110
0.014	9.7	15	0.098	0.109	0.125	0.118	0.102	0.111	0.104	0.115	0.110
0.014	9.7	20	0.109	0.115	0.078	0.089	0.122	0.112	0.115	0.119	0.107
0.014	9.7	25	0.097	0.122	0.115	0.114	0.106	0.073	0.095	0.125	0.106
0.014	9.7	30	0.068	0.098	0.071	0.070	0.074	0.068	0.062	0.071	0.073
0.019	9.7	5	0.114	0.123	0.129	0.108	0.118	0.117	0.113	0.108	0.116
0.019	9.7	10	0.108	0.115	0.109	0.111	0.115	0.112	0.111	0.113	0.112
0.019	9.7	15	0.100	0.107	0.113	0.112	0.106	0.108	0.114	0.108	0.108

APPENDIX A4: Values of the dispersed slag phase at various gas flow rates along the axis situated at 135 degrees (Bath height: 43.5 cm; radial distance =9.7 cm).

Gas flow rate m^3/s	*Radial distance* cm	*Axial distance* cm	*Meas1 Dph*	*Meas2 Dph*	*Meas3 Dph*	*Meas4 Dph*	*Meas5 Dph*	*Meas6 Dph*	*Meas7 Dph*	*Meas8 Dph*	*Av.*
0.01	9.7	5	0.103	0.123	0.122	0.108	0.126	0.094	0.121	0.117	0.114
0.01	9.7	10	0.112	0.122	0.117	0.117	0.118	0.121	0.104	0.123	0.117
0.01	9.7	15	0.103	0.110	0.099	0.113	0.125	0.109			0.110
0.01	9.7	20	0.102	0.092	0.110	0.104	0.085	0.100	0.117		0.101
0.01	9.7	25	0.083	0.056	0.077	0.074	0.069	0.065	0.103		0.075
0.01	9.7	30	0.042	0.069	0.051	0.085	0.055	0.043	0.075	0.069	0.061
0.014	9.7	5	0.119	0.114	0.112	0.103	0.108	0.106	0.113	0.112	0.111
0.014	9.7	10	0.113	0.122	0.119	0.116	0.119	0.122	0.112		0.118
0.014	9.7	15	0.120	0.109	0.112	0.117	0.119	0.111	0.111	0.112	0.114
0.014	9.7	20	0.120	0.120	0.126	0.121	0.111	0.112	0.125	0.124	0.120
0.014	9.7	25	0.109	0.109	0.108	0.101	0.107	0.100	0.107	0.119	0.107
0.014	9.7	30	0.112	0.108	0.109	0.104	0.108	0.108	0.109	0.104	0.108
0.019	9.7	5	0.109	0.115	0.115	0.123	0.119	0.118	0.104	0.113	0.115
0.019	9.7	10	0.114	0.118	0.123	0.114	0.125	0.106	0.125	0.129	0.119
0.019	9.7	15	0.108	0.114	0.111	0.111	0.111	0.111	0.111	0.113	0.111
0.019	9.7	20	0.120	0.117	0.118	0.128	0.118	0.115	0.115	0.111	0.118
0.019	9.7	25	0.112	0.121	0.120	0.115	0.120	0.113	0.115	0.118	0.117
0.019	9.7	30	0.113	0.109	0.111	0.113	0.115	0.118	0.118	0.122	0.115

Appendix A5: Values of the dispersed slag phase at various flow rates along the radial axis situated at 45 degrees (bath height: 43.5 cm)

Gas flow rate m^3/s	r cm	Axial distance cm	Meas1 Dph	Meas2 Dph	Meas3 Dph	Meas4 Dph	Meas5 Dph	Meas6 Dph	Meas7 Dph	Meas8 Dph	Av.
0.01	9.7	20	0.103	0.103	0.069	0.086	0.085	0.121	0.069	0.085	0.090
0.014	9.7	20	0.103	0.111	0.112	0.103	0.095	0.103	0.111	0.102	0.105
0.019	9.7	20	0.120	0.130	0.116	0.127	0.130	0.118	0.118	0.122	0.123
0.01	9.7	25	0.060	0.095	0.069	0.095	0.086	0.085	0.102	0.093	0.086
0.014	9.7	25	0.115	0.118	0.121	0.103	0.115	0.121	0.102	0.112	0.113
0.019	9.7	25	0.115	0.113	0.113	0.123	0.113	0.120	0.113	0.120	0.116
0.01	9.7	30	0.026	0.043	0.034	0.052	0.017	0.034	0.034	0.043	0.035
0.014	9.7	30	0.103	0.116	0.121	0.103	0.102	0.121	0.111	0.094	0.109
0.019	9.7	30	0.112	0.106	0.113	0.112	0.105	0.112	0.112	0.113	0.110
0.01	19	20	0.103	0.114	0.093	0.094	0.103	0.103	0.103	0.102	0.102
0.014	19	20	0.113	0.105	0.114	0.104	0.111	0.107	0.111	0.105	0.109
0.019	19	20	0.113	0.118	0.111	0.115	0.125	0.119	0.117	0.117	0.117
0.01	19	25	0.121	0.121	0.103	0.093	0.112	0.103	0.103	0.102	0.107
0.014	19	25	0.112	0.103	0.110	0.103	0.103	0.103	0.094	0.102	0.104
0.019	19	25	0.113	0.123	0.117	0.117	0.111	0.115	0.109	0.113	0.115
0.01	19	30	0.068	0.069	0.052	0.052	0.069	0.069	0.086	0.051	0.064
0.014	19	30	0.086	0.086	0.086	0.068	0.079	0.077	0.060	0.085	0.078
0.019	19	30	0.123	0.111	0.123	0.123	0.118	0.109	0.116	0.107	0.116

r is the radial distance

Appendix B: Values of the dispersed slag phase at various bath heights ($0.019\ m^3/s,\ z = 25\,cm$)

Bath height *cm*	*r* *cm*	Angle Degrees	Meas1 Dph	Meas2 Dph	Meas3 Dph	Meas4 Dph	Meas5 Dph	Meas6 Dph	Meas7 Dph	Meas8 Dph	Av.
43.5	9.7	45	0.115	0.113	0.113	0.123	0.113	0.120	0.113	0.120	0.116
54.6	9.7	45	0.109	0.115	0.117	0.111	0.121	0.111	0.129	0.108	0.115
65.8	9.7	45	0.114	0.111	0.109	0.105	0.106	0.114	0.114	0.106	0.110
43.5	19	45	0.113	0.123	0.117	0.117	0.111	0.115	0.109	0.113	0.115
54.6	19	45	0.121	0.118	0.115	0.103	0.097	0.121	0.117	0.119	0.114
65.8	19	45	0.1	0.103	0.103	0.108	0.108	0.108	0.111		0.106
43.5	9.7	90	0.120	0.115	0.115	0.128	0.122	0.115	0.121	0.117	0.120
54.6	9.7	90	0.129	0.133	0.131	0.119	0.119	0.121	0.107	0.131	0.124
65.8	9.7	90	0.116	0.11	0.114	0.107	0.109	0.108	0.111	0.114	0.111

Appendix C1: Numerical values of the axial dispersed slag phase on the left side (Bath height: 43.5 cm; 0.01 m^3/s)

Gas flow rate m^3/s	r cm	Axial distance cm	Meas1 Dph	Meas2 Dph	Meas3 Dph	Meas4 Dph	Meas5 Dph	Meas6 Dph	Meas7 Dph	Meas8 Dph	Av.
0.01	9.7	5	0.130	0.123	0.140	0.155	0.129	0.105	0.121	0.136	0.130
0.01	9.7	10	0.121	0.112	0.121	0.121	0.121		0.119		0.119
0.01	9.7	15	0.086	0.125	0.138	0.130	0.121	0.103	0.121	0.102	0.116
0.01	9.7	20	0.103	0.103	0.069	0.086	0.085	0.121	0.069	0.085	0.090
0.01	9.7	25	0.060	0.095	0.069	0.095	0.086	0.085	0.102	0.093	0.086
0.01	9.7	30	0.026	0.043	0.034	0.052	0.017	0.034	0.034	0.043	0.035
0.01	19	5	0.138	0.123	0.121	0.123	0.138	0.140	0.105	0.130	0.127
0.01	19	10	0.125	0.123	0.121	0.140	0.103	0.110	0.121	0.143	0.123
0.01	19	15	0.093	0.102	0.138	0.103	0.138	0.138	0.128	0.113	0.119
0.01	19	20	0.069	0.103	0.110	0.112	0.103	0.086	0.103		0.098
0.01	19	25	0.119		0.052	0.096	0.086	0.102	0.069		0.087
0.01	19	30	0.096	0.096	0.043	0.034	0.069	0.086	0.069	0.076	0.071

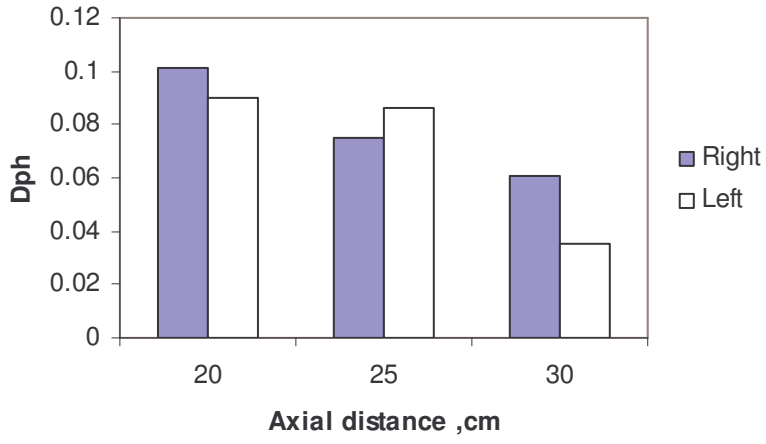

Figure 4A: comparison of the dispersed phase between right and left side of the reactor (Radial distance = 9.7 cm, gas flow rate = 0.01 m^3/s)

Appendix C2: Numerical values of the axial dispersed slag phase on the right side (Bath height: 43.5 cm; 0.01 m^3/s)

Gas flow rate m^3/s	r cm	Axial distance cm	Meas1 Dph	Meas2 Dph	Meas3 Dph	Meas4 Dph	Meas5 Dph	Meas6 Dph	Meas7 Dph	Meas8 Dph	Av.
0.01	9.7	5	0.103	0.123	0.122	0.108	0.126	0.094	0.121	0.117	0.114
0.01	9.7	10	0.112	0.122	0.117	0.119	0.118	0.121	0.104	0.123	0.117
0.01	9.7	15	0.103	0.110	0.099	0.113	0.125	0.109			0.110
0.01	9.7	20	0.102	0.092	0.110	0.104	0.085	0.100	0.117		0.101
0.01	9.7	25	0.083	0.056	0.076	0.074	0.069	0.065	0.103		0.075
0.01	9.7	30	0.042	0.069	0.051	0.085	0.055	0.043	0.075	0.068	0.061
0.01	19	5	0.089	0.101	0.100	0.104	0.109	0.108	0.095	0.082	0.099
0.01	19	10	0.107	0.095	0.103	0.089	0.082	0.103			0.097
0.01	19	15	0.103	0.088	0.087	0.109	0.103	0.088	0.084	0.086	0.094
0.01	19	20	0.085	0.086	0.096	0.077	0.087	0.087	0.086	0.105	0.089
0.01	19	25	0.095	0.095	0.085	0.089	0.069	0.102	0.094	0.077	0.088
0.01	19	30	0.103	0.103	0.102	0.077		0.069	0.086	0.103	0.094

Appendix D1: Values of the dispersed slag phase at various flow rates along the radial axis situated at 45 degrees (bath height: 54.5 cm)

Gas flow rate m^3/s	r cm	Axial distance cm	Meas1 Dph	Meas2 Dph	Meas3 Dph	Meas4 Dph	Meas5 Dph	Meas6 Dph	Meas7 Dph	Meas8 Dph	Av.
0.01	9.7	20	0.118	0.121	0.115	0.125	0.122	0.122	0.116	0.118	0.120
0.014	9.7	20	0.141	0.136	0.115	0.139	0.132	0.125	0.136	0.115	0.130
0.019	9.7	20	0.106	0.117	0.133	0.129	0.133	0.129	0.129		0.125
0.01	9.7	25	0.123	0.12	0.122	0.115	0.121	0.118	0.112	0.107	0.117
0.014	9.7	25	0.118	0.128	0.111	0.132	0.116	0.135	0.136	0.125	0.125
0.019	9.7	25	0.138	0.133	0.129	0.125	0.133	0.123	0.138		0.131
0.01	9.7	30	0.12	0.112	0.124	0.114	0.116	0.113	0.111		0.116
0.014	9.7	30	0.118	0.123	0.118	0.108	0.122	0.117	0.125	0.117	0.118
0.019	9.7	30	0.127	0.106	0.121	0.123	0.121	0.125	0.131		0.122
0.01	19	20	0.108	0.090	0.100	0.098	0.096	0.105	0.109	0.090	0.099
0.014	19	20	0.102	0.109	0.113	0.105	0.117	0.115	0.113	0.114	0.110
0.019	19	20	0.115	0.108	0.106	0.103	0.108	0.113	0.103	0.129	0.111
0.01	19	25	0.104	0.101	0.109	0.105	0.092	0.104	0.109	0.104	0.104
0.014	19	25	0.111	0.114	0.114	0.111	0.114	0.117	0.113	0.108	0.117
0.019	19	25	0.113	0.103	0.120	0.119	0.102	0.119	0.097		0.110
0.01	19	30	0.09	0.089	0.092	0.083	0.092	0.105	0.093	0.092	0.092
0.014	19	30	0.114	0.117	0.105	0.117	0.107	0.100	0.109	0.103	0.109
0.019	19	30	0.103	0.113	0.119	0.100	0.099	0.115	0.109	0.111	0.109

Appendix D2: Values of the dispersed slag phase at various flow rates along the radial axis situated at 135 degrees (bath height: 54.5 cm) on the left side

Gas flow rate m^3/s	r cm	Axial distance cm	Meas1 Dph	Meas2 Dph	Meas3 Dph	Meas4 Dph	Meas5 Dph	Meas6 Dph	Meas7 Dph	Meas8 Dph	Av.
0.01	9.7	20	0.131	0.130	0.122	0.129	0.125	0.118	0.111	0.128	0.124
0.014	9.7	20	0.121	0.130	0.132	0.121	0.138	0.123	0.122	0.118	0.126
0.019	9.7	20	0.129	0.113	0.113	0.121	0.133	0.133	0.119	0.117	0.122
0.01	9.7	25	0.132	0.119	0.125	0.108	0.119	0.129	0.120	0.133	0.123
0.014	9.7	25	0.108	0.125	0.120	0.116	0.108	0.118	0.126	0.115	0.117
0.019	9.7	25	0.133	0.133	0.121	0.111	0.129	0.121	0.119	0.125	0.124
0.01	9.7	30	0.104	0.118	0.114	0.104	0.111	0.111	0.121	0.118	0.113
0.014	9.7	30	0.100	0.120	0.116	0.119	0.114	0.115	0.111	0.119	0.114
0.019	9.7	30	0.113	0.119	0.121	0.121	0.121	0.127	0.129	0.133	0.123
0.01	19	20	0.105	0.106	0.107	0.109	0.119	0.116	0.117		0.111
0.014	19	20	0.101	0.119	0.109	0.122	0.119	0.109	0.106	0.114	0.113
0.019	19	20	0.118	0.106	0.131	0.123	0.133	0.111	0.131		0.122
0.01	19	25	0.102	0.101	0.109	0.100	0.095	0.114	0.109		0.105
0.014	19	25	0.107	0.100	0.100	0.118	0.106	0.09	0.110	0.111	0.105
0.019	19	25	0.113	0.121	0.125	0.119	0.108	0.111	0.117	0.119	0.116
0.01	19	30	0.115	0.116	0.102	0.088	0.093	0.100	0.083	0.100	0.099
0.014	19	30	0.08	0.106	0.100	0.067	0.100	0.114	0.119	0.111	0.100
0.019	19	30	0.117	0.109	0.095	0.119	0.121	0.125	0.094	0.133	0.114

Appendix D3: Values of the dispersed slag phase at various flow rates along the radial axis situated at 90 degrees (bath height: 54.5 cm) on the left side

Gas flow rate m^3/s	r cm	Axial distance cm	Meas1 Dph	Meas2 Dph	Meas3 Dph	Meas4 Dph	Meas5 Dph	Meas6 Dph	Meas7 Dph	Meas8 Dph	Av.
0.01	9.7	20	0.111	0.119	0.125	0.125	0.129	0.121	0.119	0.122	0.121
0.014	9.7	20	0.125	0.112	0.103	0.125	0.111	0.109	0.118	0.113	0.114
0.019	9.7	20	0.125	0.138	0.125	0.123	0.121	0.125	0.138		0.128
0.01	9.7	25	0.125	0.131	0.125	0.131	0.108	0.125	0.121	0.120	0.123
0.014	9.7	25	0.117	0.109	0.117	0.133	0.118	0.131	0.115	0.111	0.119
0.019	9.7	25	0.137	0.121	0.117	0.125	0.121	0.133	0.121		0.125
0.01	9.7	30	0.105	0.119	0.118	0.103	0.113	0.100	0.118	0.105	0.110
0.014	9.7	30	0.133	0.117	0.150	0.125	0.121	0.131	0.130	0.152	0.132
0.019	9.7	30	0.129	0.129	0.125	0.133	0.121	0.104	0.133	0.125	0.125
0.01	19	20	0.116	0.114	0.107	0.098	0.100	0.109	0.116	0.093	0.106
0.014	19	20	0.094	0.096	0.111	0.105	0.114	0.111	0.120	0.100	0.106
0.019	19	20	0.090	0.113	0.095	0.100	0.106	0.100	0.103	0.113	0.103
0.01	19	25	0.100	0.105	0.101	0.103	0.111	0.103	0.106	0.107	0.104
0.014	19	25	0.100	0.106	0.106	0.103	0.111	0.090	0.113	0.099	0.104
0.019	19	25	0.111	0.113	0.096	0.098	0.111	0.119	0.113		0.109
0.01	19	30	0.109	0.105	0.112	0.096	0.090	0.106	0.098	0.109	0.103
0.014	19	30	0.100	0.111	0.117	0.104	0.096	0.098	0.106	0.090	0.103
0.019	19	30	0.116	0.115	0.111	0.103	0.109	0.119	0.103	0.106	0.110

Appendix D4: Values of the dispersed slag phase at various radial axis (bath height: 54.5cm; gas flow rate: 0.01 m^3/s; right side)

Radial Axis Angle (degrees)	*r* *cm*	Axial distance *cm*	Meas1 Dph	Meas2 Dph	Meas3 Dph	Meas4 Dph	Meas5 Dph	Meas6 Dph	Meas7 Dph	Meas8 Dph	Av.
45	9.7	20	0.111	0.116	0.112	0.120	0.117	0.100	0.112	0.100	0.111
90	9.7	20	0.122	0.122	0.112	0.109	0.114	0.113	0.122	0.113	0.116
135	9.7	20	0.111	0.120	0.120	0.123	0.120	0.120	0.126		0.120
45	9.7	25	0.122	0.116	0.112	0.127	0.109	0.117	0.114	0.090	0.114
90	9.7	25	0.111	0.125	0.111	0.120	0.122	0.119	0.118	0.125	0.119
135	9.7	25	0.123	0.125	0.126	0.129	0.126	0.123	0.127		0.126
45	9.7	30	0.116	0.120	0.122	0.118	0.115	0.130	0.107	0.120	0.119
90	9.7	30	0.118	0.117	0.117	0.115	0.122	0.120	0.111		0.117
135	9.7	30	0.123	0.113	0.122	0.119	0.122	0.113	0.115	0.127	0.119
45	19	20	0.108	0.108	0.114	0.102	0.098	0.104	0.107	0.118	0.107
90	19	20	0.106	0.105	0.109	0.114	0.117	0.109	0.118	0.098	0.109
135	19	20	0.109	0.113	0.113	0.110	0.098	0.117	0.122	0.102	0.110
45	19	25	0.106	0.111	0.114	0.106	0.109	0.108	0.114	0.098	0.108
90	19	25	0.117	0.122	0.120	0.122	0.122	0.109	0.115	0.120	0.119
135	19	25	0.111	0.119	0.107	0.118	0.102	0.117	0.120	0.115	0.114
45	19	30	0.103	0.114	0.110	0.120	0.105	0.115	0.104	0.096	0.108
90	19	30	0.116	0.118	0.120	0.120	0.112	0.117	0.118	0.117	0.117
135	19	30	0.107	0.114	0.129	0.132	0.113	0.118	0.122		0.119

Appendix D5: Values of the dispersed slag phase at various radial axis (bath height: 54.5cm; gas flow rate: 0.014 m^3/s; right side)

Radial Axis Angle (degrees)	*r* *cm*	Axial distance *cm*	Meas1 Dph	Meas2 Dph	Meas3 Dph	Meas4 Dph	Meas5 Dph	Meas6 Dph	Meas7 Dph	Meas8 Dph	Av.
45	9.7	20	0.111	0.109	0.122	0.116	0.109	0.116	0.111	0.111	0.113
90	9.7	20	0.107	0.108	0.118	0.111	0.109	0.118	0.116	0.106	0.112
135	9.7	20	0.114	0.115	0.119	0.111	0.118	0.125	0.113	0.112	0.116
45	9.7	25	0.112	0.114	0.118	0.109	0.115	0.131	0.111	0.115	0.116
90	9.7	25	0.108	0.119	0.111	0.105	0.125	0.122	0.119	0.114	0.115
135	9.7	25	0.117	0.116	0.117	0.113	0.125	0.123	0.115	0.114	0.118
45	9.7	30	0.116	0.123	0.114	0.116	0.117	0.125	0.116	0.114	0.118
90	9.7	30	0.125	0.112	0.119	0.116	0.111	0.100	0.118	0.105	0.113
135	9.7	30	0.130	0.127	0.128	0.120	0.117	0.127	0.126	0.122	0.125
45	19	20	0.111	0.119	0.122	0.115	0.116	0.113	0.114	0.108	0.115
90	19	20	0.118	0.120	0.109	0.116	0.118	0.116	0.117	0.111	0.116
135	19	20	0.119	0.117	0.118	0.118	0.106	0.113	0.094	0.114	0.112
45	19	25	0.109	0.113	0.118	0.112	0.109	0.116	0.109	0.114	0.113
90	19	25	0.113	0.120	0.118	0.111	0.113	0.113	0.108	0.116	0.114
135	19	25	0.108	0.114	0.128	0.119	0.111	0.114	0.119	0.123	0.117
45	19	30	0.111	0.119	0.115	0.105	0.113	0.116	0.122	0.111	0.114
90	19	30	0.117	0.114	0.108	0.106	0.107	0.123	0.121	0.117	0.114
135	19	30	0.111	0.125	0.121	0.122	0.113	0.122	0.129	0.120	0.120

Appendix D6: Values of the dispersed slag phase at various radial axis (bath height: 54.5cm; gas flow rate: 0.019 m^3/s; right side)

Radial Axis Angle (degrees)	*r* *cm*	Axial distance *cm*	Meas1 Dph	Meas2 Dph	Meas3 Dph	Meas4 Dph	Meas5 Dph	Meas6 Dph	Meas7 Dph	Meas8 Dph	Av.
45	9.7	20	0.108	0.113	0.114	0.117	0.109	0.138	0.121	0.115	0.117
90	9.7	20	0.118	0.121	0.123	0.121	0.121	0.122	0.115		0.120
135	9.7	20	0.115	0.115	0.125	0.117	0.121	0.125	0.117	0.121	0.119
45	9.7	25	0.109	0.115	0.117	0.111	0.121	0.111	0.129	0.108	0.115
90	9.7	25	0.137	0.121	0.117	0.125	0.121	0.133	0.121		0.124
135	9.7	25	0.113	0.118	0.117	0.133	0.123	0.125	0.117	0.121	0.121
45	9.7	30	0.133	0.125	0.113	0.138	0.121	0.119	0.115	0.115	0.122
90	9.7	30	0.129	0.129	0.125	0.133	0.121	0.104	0.133	0.125	0.125
135	9.7	30	0.121	0.121	0.123	0.118	0.133	0.133	0.127	0.129	0.126
45	19	20	0.101	0.103	0.103	0.107	0.103	0.115	0.103	0.103	0.105
90	19	20	0.121	0.117	0.125	0.123	0.117	0.129	0.133	0.133	0.125
135	19	20	0.097	0.100	0.109	0.133	0.100	0.119	0.133	0.115	0.113
45	19	25	0.120	0.119	0.115	0.103	0.097	0.121	0.117	0.119	0.114
90	19	25	0.137	0.133	0.113	0.122	0.113	0.112	0.133	0.117	0.124
135	19	25	0.129	0.111	0.115	0.133	0.129	0.119	0.125	0.115	0.122
45	19	30	0.120	0.119	0.100	0.138	0.121	0.118	0.107	0.119	0.118
90	19	30	0.127	0.137	0.129	0.129	0.109	0.115	0.119	0.109	0.122
135	19	30	0.127	0.111	0.129	0.121	0.125	0.109			0.120

Figure 3F: Fluid flow in the CLU model

Figure 3G: Air flow rate equipment for the CLU model

Appendix E1: Values of the dispersed slag phase at various radial axis (bath height: 65.9cm; gas flow rate: 0.019 m^3/s; left side)

Radial Axis Angle (degrees)	*r* *cm*	Axial distance *cm*	Meas1 Dph	Meas2 Dph	Meas3 Dph	Meas4 Dph	Meas5 Dph	Meas6 Dph	Meas7 Dph	Meas8 Dph	Av.
45	9.7	20	0.116	0.111	0.116	0.112	0.111	0.119	0.113	0.109	0.113
90	9.7	20	0.116	0.109	0.108	0.121	0.117	0.111	0.114	0.113	0.114
135	9.7	20	0.119	0.111	0.111	0.114	0.115	0.116	0.106		0.113
45	9.7	25	0.128	0.131	0.122	0.113	0.125	0.123	0.122	0.122	0.123
90	9.7	25	0.109	0.111	0.103	0.103	0.118	0.114	0.120	0.102	0.110
135	9.7	25	0.114	0.117	0.114	0.112	0.125	0.122	0.112		0.117
45	9.7	30	0.111	0.119	0.119	0.136	0.116	0.106	0.107	0.108	0.115
90	9.7	30	0.111	0.119	0.119	0.136	0.116	0.106	0.107	0.108	0.115
135	9.7	30	0.102	0.105	0.111	0.106	0.122	0.106	0.119	0.108	0.110
45	19	20	0.107	0.103	0.111	0.108	0.114	0.111	0.103	0.114	0.109
90	19	20	0.107	0.103	0.111	0.108	0.114	0.111	0.103	0.114	0.109
135	19	20	0.114	0.119	0.113	0.125	0.122	0.120	0.109	0.122	0.118
45	19	25	0.108	0.090	0.106	0.103	0.114	0.118	0.104	0.115	0.107
90	19	25	0.108	0.090	0.106	0.103	0.114	0.118	0.104	0.115	0.107
135	19	25	0.111	0.100	0.113	0.107	0.105	0.119	0.111	0.103	0.109
45	19	30	0.099	0.100	0.109	0.107	0.101	0.102	0.104	0.100	0.103
90	19	30	0.108	0.117	0.103	0.118	0.114	0.111	0.100	0.108	0.110
135	19	30	0.108	0.118	0.103	0.118	0.114	0.111	0.100	0.108	0.110

Appendix E2: Values of the dispersed slag phase at various radial axis

(Bath height: 65.9 cm; gas flow rate: 0.019 m^3/s; right side)

Radial Axis Angle (degrees)	*r* *cm*	Axial distance *cm*	Meas1 Dph	Meas2 Dph	Meas3 Dph	Meas4 Dph	Meas5 Dph	Meas6 Dph	Meas7 Dph	Meas8 Dph	Av.
45	9.7	20	0.108	0.103	0.108	0.108	0.106	0.113	0.100	0.105	0.106
90	9.7	20	0.118	0.114	0.122	0.117	0.103	0.118	0.114	0.111	0.115
135	9.7	20	0.116	0.117	0.116	0.103	0.109	0.118	0.108	0.118	0.113
45	9.7	25	0.114	0.111	0.108	0.105	0.106	0.114	0.113	0.106	0.110
90	9.7	25	0.116	0.110	0.114	0.107	0.108	0.108	0.111	0.114	0.111
135	9.7	25	0.111	0.111	0.103	0.114	0.111	0.113	0.116	0.118	0.112
45	9.7	30	0.113	0.110	0.112	0.114	0.119	0.118	0.113	0.118	0.115
90	9.7	30	0.113	0.109	0.119	0.111	0.106	0.111	0.115		0.112
135	9.7	30	0.111	0.117	0.117	0.116	0.113	0.125			0.117
45	19	20	0.107	0.110	0.098	0.105	0.100	0.113	0.109	0.113	0.107
90	19	20	0.115	0.111	0.106	0.109	0.114	0.100	0.106	0.113	0.109
135	19	20	0.101	0.106	0.118	0.104	0.097	0.103	0.103		0.104
45	19	25	0.100	0.103	0.102	0.108	0.108	0.108	0.111		0.106
90	19	25	0.118	0.108	0.111	0.111	0.105	0.111	0.102	0.100	0.108
135	19	25	0.102	0.111	0.111	0.116	0.118	0.109	0.121	0.105	0.112
45	19	30	0.103	0.111	0.111	0.115	0.115	0.116	0.105	0.112	0.111
90	19	30	0.113	0.109	0.119	0.111	0.106	0.111	0.115		0.112
135	19	30	0.113	0.106	0.110	0.105	0.110	0.095	0.100	0.097	0.104

Appendix F1: Fitting information

Data Fit version 8.1.69

Results from project "Untitled1"

Equation ID: bifuraha1

Model Definition:

F1 = 1-x^2

F2 = F1^b

Y = a*F2

Number of observations = 3

Number of missing observations = 0

Solver type: Nonlinear

Nonlinear iteration limit = 250

Diverging nonlinear iteration limit =10

Number of nonlinear iterations performed = 9

Residual tolerance = 0.0000000001

Sum of Residuals = 2.632E-07

Average Residual = 8.770E-08

Residual Sum of Squares (Absolute) = 4.41E-07

Residual Sum of Squares (Relative) = 4.410E-07

Standard Error of the Estimate = 6.641E-04

Coefficient of Multiple Determination (R^2) = 0.989

Proportion of Variance Explained = 98.935%

Adjusted coefficient of multiple determination (Ra^2) = 0.9787

Durbin-Watson statistic = 2.84686325597767

Regression Variable Results

Variable	Value	Standard Error	t-ratio
a	0.121	5.37E-04	226.1
b	0.290	3.03E-02	9.55

F2: Fitting information

Data Fit version 8.1.69

Results from project "Untitled1"

Equation ID: bifuraha1

Model Definition:

F1 = 1-x^2

F2 = F1^b

Y = a*F2

Number of observations = 3

Number of missing observations = 0

Solver type: Nonlinear

Nonlinear iteration limit = 250

Diverging nonlinear iteration limit =10

Number of nonlinear iterations performed = 3

Residual tolerance = 0.0000000001

Sum of Residuals = -9.374E-07

Average Residual = -3.125E-07

Residual Sum of Squares (Absolute) = 1.76E-06

Residual Sum of Squares (Relative) = 1.76E-06

Standard Error of the Estimate = 1.329E-03

Coefficient of Multiple Determination (R^2) = 0.973

Proportion of Variance Explained = 97.3%

Adjusted coefficient of multiple determination (Ra^2) = 0.946

Durbin-Watson statistic = 2.852

Regression Variable Results

Variable	Value	Standard Error	t-ratio
a	0.115	1.08E-03	106.76
b	0.386	6.52E-02	5.9192

F3: Fitting information

Data Fit version 8.1.69

Results from project "Untitled1"

Equation ID: bifuraha1

Model Definition:

F1 = 1-x^2

F2 = F1^b

Y = a*F2

Number of observations = 3

Number of missing observations = 0

Solver type: Nonlinear

Nonlinear iteration limit = 250

Diverging nonlinear iteration limit =10

Number of nonlinear iterations performed = 3

Residual tolerance = 0.0000000001

Sum of Residuals = -3.479E-08

Average Residual = -1.159E-08

Residual Sum of Squares (Absolute) = 4.365E-08

Residual Sum of Squares (Relative) = 4.365E-08

Standard Error of the Estimate = 2.089E-04

Coefficient of Multiple Determination (R^2) = 0.997

Proportion of Variance Explained = 99.7%

Adjusted coefficient of multiple determination (Ra^2) = 0.994

Durbin-Watson statistic = 2.841

Regression Variable Results

Variable	Value	Standard Error	t-ratio
a	0.114	1.685E-04	676.4
b	0.188	1.000E-02	18.9

F4: Fitting information

Data Fit version 8.1.69

Results from project "Untitled1"

Equation ID: bifuraha1

Model Definition:

F1 = 1-x^2

F2 = F1^b

Y = a*F2

Number of observations = 3

Number of missing observations = 0

Solver type: Nonlinear

Nonlinear iteration limit = 250

Diverging nonlinear iteration limit =10

Number of nonlinear iterations performed = 3

Residual tolerance = 0.0000000001

Sum of Residuals = -3.717E-06

Average Residual = -1.239E-06

Residual Sum of Squares (Absolute) = 3.104E-06

Residual Sum of Squares (Relative) = 3.104E-06

Standard Error of the Estimate = 1.762E-03

Coefficient of Multiple Determination (R^2) = 0.978

Proportion of Variance Explained = 97.8%

Adjusted coefficient of multiple determination (Ra^2) = 0.955

Durbin-Watson statistic = 2.867

Regression Variable Results

Variable	Value	Standard Error	t-ratio
a	0.101	1.438E-03	70.4
b	0.663	0.103	6.4

F5: Fitting information

Data Fit version 8.1.69

Results from project "Untitled1"

Equation ID: bifuraha1

Model Definition:

F1 = 1-x^2

F2 = F1^b

Y = a*F2

Number of observations = 3

Number of missing observations = 0

Solver type: Nonlinear

Nonlinear iteration limit = 250

Diverging nonlinear iteration limit =10

Number of nonlinear iterations performed = 3

Residual tolerance = 0.0000000001

Sum of Residuals = -2.240E-06

Average Residual = -7.468E-07

Residual Sum of Squares (Absolute) = 6.013E-06

Residual Sum of Squares (Relative) = 6.013E-06

Standard Error of the Estimate = 2.452E-03

Coefficient of Multiple Determination (R^2) = 0.933

Proportion of Variance Explained = 93.3%

Adjusted coefficient of multiple determination (Ra^2) = 0.867

Durbin-Watson statistic = 2.855

Regression Variable Results

Variable	Value	Standard Error	t-ratio
a	0.117	1.990E-03	59.9
b	0.439	0.119	3.68

F6: Fitting information

Data Fit version 8.1.69

Results from project "Untitled1"

Equation ID: bifuraha1

Model Definition:

F1 = 1-x^2

F2 = F1^b

Y = a*F2

Number of observations = 3

Number of missing observations = 0

Solver type: Nonlinear

Nonlinear iteration limit = 250

Diverging nonlinear iteration limit =10

Number of nonlinear iterations performed = 3

Residual tolerance = 0.0000000001

Sum of Residuals = -8.950E-07

Average Residual = -2.983E-07

Residual Sum of Squares (Absolute) = 3.310E-07

Residual Sum of Squares (Relative) = 3.310E-07

Standard Error of the Estimate = 5.753E-04

Coefficient of Multiple Determination (R^2) = 0.997

Proportion of Variance Explained = 99.7%

Adjusted coefficient of multiple determination (Ra^2) = 0.995

Durbin-Watson statistic = 2.861

Regression Variable Results

Variable	Value	Standard Error	t-ratio
a	0.113	4.685E-04	241.5
b	0.570	2.965E-02	19.2

F7: Fitting information

Data Fit version 8.1.69

Results from project "Untitled1"

Equation ID: bifuraha1

Model Definition:

F1 = 1-x^2

F2 = F1^b

Y = a*F2

Number of observations = 3

Number of missing observations = 0

Solver type: Nonlinear

Nonlinear iteration limit = 250

Diverging nonlinear iteration limit =10

Number of nonlinear iterations performed = 3

Residual tolerance = 0.0000000001

Sum of Residuals = -1.845E-06

Average Residual = -6.151E-07

Residual Sum of Squares (Absolute) = 4.652E-06

Residual Sum of Squares (Relative) = 4.652E-06

Standard Error of the Estimate = 2.157E-03

Coefficient of Multiple Determination (R^2) = 0.937

Proportion of Variance Explained = 93.7%

Adjusted coefficient of multiple determination (Ra^2) = 0.873

Durbin-Watson statistic = 2.854

Regression Variable Results

Variable	Value	Standard Error	t-ratio
a	0.109	1.750E-03	62.5
b	0.425	0.112	3.8

F8: Fitting information

Data Fit version 8.1.69

Results from project "Untitled1"

Equation ID: bifuraha1

Model Definition:

F1 = 1-x^2

F2 = F1^b

Y = a*F2

Number of observations = 3

Number of missing observations = 0

Solver type: Nonlinear

Nonlinear iteration limit = 250

Diverging nonlinear iteration limit =10

Number of nonlinear iterations performed = 3

Residual tolerance = 0.0000000001

Sum of Residuals = -4.107E-08

Average Residual = -1.369E-08

Residual Sum of Squares (Absolute) = 1.675E-07

Residual Sum of Squares (Relative) = 1.675E-07

Standard Error of the Estimate = 4.09E-04

Coefficient of Multiple Determination (R^2) = 0.983

Proportion of Variance Explained = 98.3%

Adjusted coefficient of multiple determination (Ra^2) = 0.967

Durbin-Watson statistic = 2.839

Regression Variable Results

Variable	Value	Standard Error	t-ratio
a	0.115	3.298E-04	350.1
b	0.146	1.922E-02	7.6

F9: Fitting information

Data Fit version 8.1.69

Results from project "Untitled1"

Equation ID: bifuraha1

Model Definition:

F1 = 1-x^2

F2 = F1^b

Y = a*F2

Number of observations = 3

Number of missing observations = 0

Solver type: Nonlinear

Nonlinear iteration limit = 250

Diverging nonlinear iteration limit =10

Number of nonlinear iterations performed = 3

Residual tolerance = 0.0000000001

Sum of Residuals = 1.300E-08

Average Residual = 4.333E-09

Residual Sum of Squares (Absolute) = 1.837E-08

Residual Sum of Squares (Relative) = 1.837E-08

Standard Error of the Estimate = 1.356E-04

Coefficient of Multiple Determination (R^2) = 0.998

Proportion of Variance Explained = 99.8%

Adjusted coefficient of multiple determination (Ra^2) = 0.996

Durbin-Watson statistic = 2.838

Regression Variable Results

Variable	Value	Standard Error	t-ratio
a	0.116	1.092E-04	1061.1
b	0.143	6.33E-03	22.6

Appendix G: Surface mapping system (win 32)

The software Surfer32 has been used in the plotting of the dispersed phase contours.

Description

Open the file Surf by double click

Open a new file, three options appear .Then, click on worksheet to open that file.

Fill in data of the radial distance, axial distance and the corresponding value of the dispersed phase

Save that worksheet and close it.

Thereafter, open a new file and select Plot

Click on the command map and select contours

In that option, select the file where the previous worksheet has been saved.

Click on ok, the dispersed phase contour appears

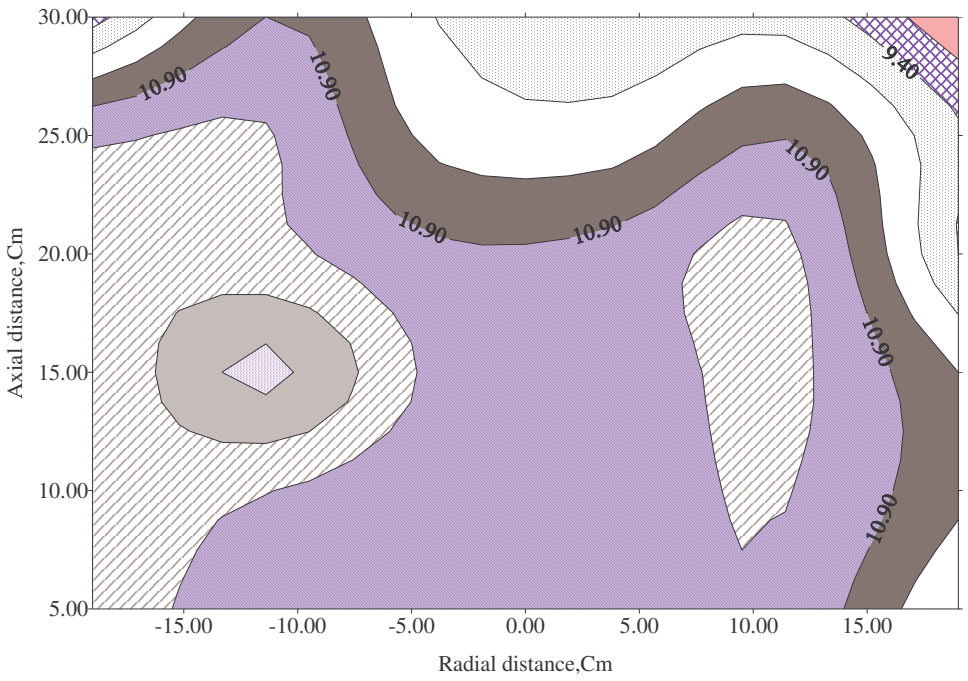

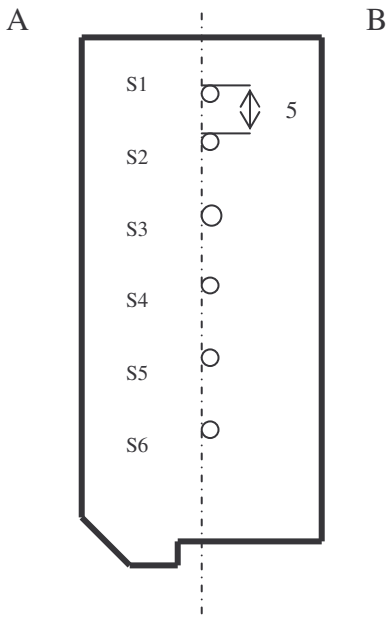

Figure 5C: Sampling points along the axial centerline

AB: original interface between the liquid phases